

RESEARCH ARTICLE

# Oxygen Isotope Variability within *Nautilus* Shell Growth Bands

Benjamin J. Linzmeier<sup>1☯\*</sup>, Reinhard Kozdon<sup>2,3☯</sup>, Shanan E. Peters<sup>1☯</sup>, John W. Valley<sup>1,3☯</sup>

**1** Department of Geoscience, University of Wisconsin-Madison, Madison, Wisconsin, United States of America, **2** Lamont-Doherty Earth Observatory, Columbia University, Palisades, New York, United States of America, **3** WiscSIMS, Department of Geoscience, University of Wisconsin-Madison, Madison, Wisconsin, United States of America

☯ These authors contributed equally to this work.

\* [blinzmeier@wisc.edu](mailto:blinzmeier@wisc.edu)



**OPEN ACCESS**

**Citation:** Linzmeier BJ, Kozdon R, Peters SE, Valley JW (2016) Oxygen Isotope Variability within *Nautilus* Shell Growth Bands. PLoS ONE 11(4): e0153890. doi:10.1371/journal.pone.0153890

**Editor:** Steffen Kiel, Naturhistoriska riksmuseet, SWEDEN

**Received:** January 11, 2016

**Accepted:** April 5, 2016

**Published:** April 21, 2016

**Copyright:** © 2016 Linzmeier et al. This is an open access article distributed under the terms of the [Creative Commons Attribution License](https://creativecommons.org/licenses/by/4.0/), which permits unrestricted use, distribution, and reproduction in any medium, provided the original author and source are credited.

**Data Availability Statement:** All relevant data are within the paper and its Supporting Information files.

**Funding:** Funding for this study came from the Geoscience Department at UW-Madison, Sigma Xi, and the U.S. Department of Energy Office of Science, Office of Basic Energy Sciences under Award Number DE-FG02-93ER14389. WiscSIMS is partially supported by the National Science Foundation (EAR-1053466 and -1355590). The funders had no role in study design, data collection and analysis, decision to publish, or preparation of the manuscript.

**Competing Interests:** The authors have declared that no competing interests exist.

## Abstract

*Nautilus* is often used as an analogue for the ecology and behavior of extinct externally shelled cephalopods. *Nautilus* shell grows quickly, has internal growth banding, and is widely believed to precipitate aragonite in oxygen isotope equilibrium with seawater. Pieces of shell from a wild-caught *Nautilus macromphalus* from New Caledonia and from a *Nautilus belauensis* reared in an aquarium were cast in epoxy, polished, and then imaged. Growth bands were visible in the outer prismatic layer of both shells. The thicknesses of the bands are consistent with previously reported daily growth rates measured in aquarium reared individuals. *In situ* analysis of oxygen isotope ratios using secondary ion mass spectrometry (SIMS) with 10 μm beam-spot size reveals inter- and intra-band δ<sup>18</sup>O variation. In the wild-caught sample, a traverse crosscutting 45 growth bands yielded δ<sup>18</sup>O values ranging 2.5‰, from +0.9 to -1.6‰ (VPDB), a range that is larger than that observed in many serial sampling of entire shells by conventional methods. The maximum range within a single band (~32 μm) was 1.5‰, and 27 out of 41 bands had a range larger than instrumental precision (±2 SD = 0.6‰). The results from the wild individual suggest depth migration is recorded by the shell, but are not consistent with a simple sinusoidal, diurnal depth change pattern. To create the observed range of δ<sup>18</sup>O, however, this *Nautilus* must have traversed a temperature gradient of at least ~12°C, corresponding to approximately 400 m depth change. Isotopic variation was also measured in the aquarium-reared sample, but the pattern within and between bands likely reflects evaporative enrichment arising from a weekly cycle of refill and replacement of the aquarium water. Overall, this work suggests that depth migration behavior in ancient nektonic mollusks could be elucidated by SIMS analysis across individual growth bands.

## Introduction

Stable carbon and oxygen isotope analyses have been used to understand living *Nautilus* ecology [1–6] and to infer the ecology of extinct externally shelled cephalopods [7–11]. Data from aquarium rearing suggest that *Nautilus*, like many mollusks, precipitate their shells in oxygen

isotope equilibrium with ambient temperature and seawater  $\delta^{18}\text{O}$  [12,13]. In the modern ocean, both the temperature and the oxygen isotope ratio of water vary with depth and seasons; however, strong seasonality is not present in low-latitude *Nautilus* habitat [14,15]. Many authors have argued that  $\delta^{18}\text{O}$  change in large samples of wild-caught *Nautilus* shell are a change in average living depth through time [1,2,8,11,12].

*Nautilus* are active swimmers that traverse hundreds of meters water depth during the day within the steep forereef environment in search of food and to avoid predators [16–19]. Photocapture traps have demonstrated that whole populations migrate several hundred meters through the water column daily [20]. Individual *Nautilus* have been tracked with remote telemetry crossing depths from >200 m to <50 m, spanning a range in water temperature of over 3°C, within individual days [17–19]. If shell precipitation is continuous across all depths in a migrating *Nautilus*, a change in  $\delta^{18}\text{O}$  should be observed within a single day's shell growth in a wild-caught individual.

Most stable isotope studies to date have used phosphoric acid digestion coupled with gas-source mass spectrometry and therefore used relatively large volume samples (>40  $\mu\text{g}$  of powder) that were collected by drilling or mechanical removal of chips (e.g. [1]). Thus, traditional methods must average multiple days of growth when extracting a sample, which precludes the detection of all short-term depth migration behavior and instead provides an average temperature for the duration of growth sampled. One study by Oba et al. [2] used finer scale physical sampling within septa that grow to full thickness over ~2 months [21]. They planed material parallel to the septal surface with the aid of a binocular microscope and interpreted oxygen isotope variability in its shell to record daily depth migration behavior, but did not relate oxygen isotope variability to banding within the septa. Therefore, the data were unconstrained in time. The external spiral could not be sampled in such a manner to resolve depth migration because growth bands are inclined relative to the outer surface (Fig 1).

Mollusk shells are composed of two major layers: the outer prismatic layer (also known as the spherulitic prismatic layer [23]), positioned away from the chamber containing the body of the mollusk, and the inner nacreous layer that lines the body chamber [24] (Fig 1). The inner nacreous layer is composed of thin (<1  $\mu\text{m}$ ) interlocking tablets of aragonite that are surrounded by an organic framework. In *Nautilus*, the nacreous layer grows at a very shallow angle relative to the outer shell surface causing growth banding within it to be very thin [25] (Fig 1). The outer prismatic layer is composed of larger interlocking crystals of aragonite that has growth banding that forms at a higher angle relative to the outer shell wall, causing banding to be thicker and therefore permitting SIMS sampling within bands [25] (Fig 1). Growth of both the prismatic and nacreous layers in *Nautilus* shell occurs in the space enclosed by the mantle and periostracum at the apertural margin [23].

Growth banding with a variety of periods is widespread in biogenic carbonates. Circadian rhythms appear deep in the tree of life [26] and modulate metabolic processes related to growth [27]. Daily growth banding and variation of growth band width have previously been reported from several other mollusks. Intraprismatic banding in gastropod mollusks is daily and isochronous across the prismatic layer [28–30]. Stalolith growth banding is daily in *Loliginidae* [31] and widths co-vary with food abundance [32]. Growth banding in bivalves has been widely studied [30,33–37]. Bivalves have daily growth banding and widths are modulated by seasonal temperature change, age, food availability and tides [29,30,38]. Growth banding in externally shelled cephalopod mollusks has only received minor attention and the periodicity and width of growth banding within the prismatic layer has not been reported for *Nautilus* [23,39–42]. External growth bands (i.e. those visible on the outer surface of the shell) in *Nautilus* are added every two days and have widths of twice that of measured daily growth rates [25,42]. External growth banding is visible in patterns of surface topography, while internal growth banding is visible due to changes in the ratio of organic matter to carbonate in the shell

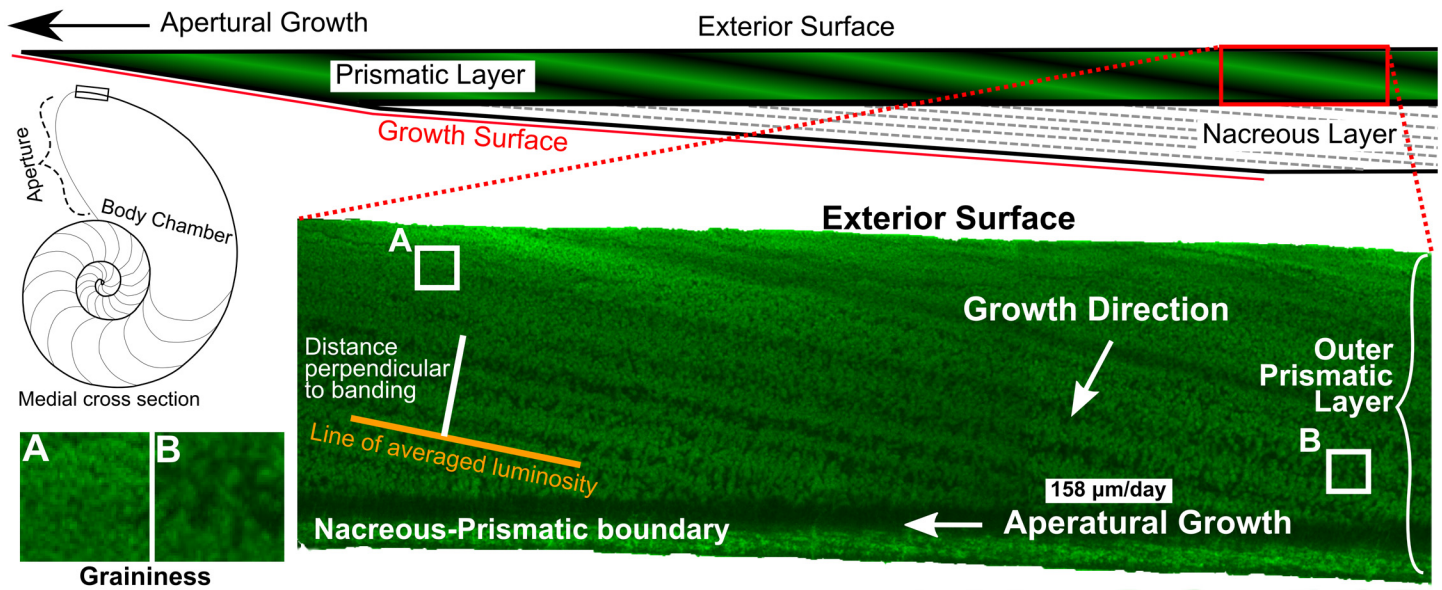


**Fig 1. Schematic illustrations of a cut through the medial plane of a *Nautilus* and full thickness shell wall at the aperture and CLFM image of *Nautilus* shell showing inclined banding visible by CLFM in the outer prismatic layer relative to actively growing surface of the shell.** SIMS measurements in this study were only from the outer prismatic layer of shell and no analyses are reported from the nacreous layer because growth banding in the nacreous layer is too thin for depth migration to be subsampled by 10- $\mu\text{m}$  SIMS spots. The CLFM image shows only the outer prismatic layer of the *Nautilus* shell. Growth bands were formed in the layer parallel to the growth surface and are likely expressed due to differences in the proportion of aragonite to intercrystalline organic matter [22]. Growth bands extend from the exterior surface of the shell to the nacreous-prismatic boundary and are inclined by  $\sim 11^\circ$  to the exterior surface. Growth rates in literature (averaging 158  $\mu\text{m}/\text{day}$  as represented by the scale bar) are typically reported as apertural growth per day, which corresponds to the distance along the exterior surface in the figure [21]. There are three major patterns within growth bands: 1) There is less contrast between the light and dark portions of bands near the exterior surface. 2) Near the exterior surface spots of brightly luminescing aragonite are small and surrounded by small spots of less luminescing aragonite (less graininess) (A). 3) Near the nacreous-prismatic boundary there are larger spots of brightly luminescing aragonite surrounded by continuous areas that do not luminesce as brightly (B). The intensity of fluorescence was measured along the distance perpendicular to banding by averaging lines of pixels parallel to growth banding.

doi:10.1371/journal.pone.0153890.g001

[22,23,43]. Growth banding visible within the outer prismatic layer of *Nautilus* shell is likely to form daily because of similarity in structure to daily growth bands in other mollusks and circadian rhythms are widespread in the tree of life.

This study investigates high spatial (10- $\mu\text{m}$  scale) and high temporal resolution (sub-daily) oxygen isotope variation in *Nautilus* shell. We relate *in situ*  $\delta^{18}\text{O}$  variability to daily growth banding imaged in the outer prismatic layer of *Nautilus* shell. We sampled one wild-caught *Nautilus macromphalus* from New Caledonia and one aquarium-reared *Nautilus belauensis* [12,44] using a secondary ion mass spectrometer (SIMS) to measure  $\delta^{18}\text{O}$  in sampling spots with high precision ( $\sim 0.3\text{‰}$  2SD). The high spatial resolution allows us to test for the record of depth-migration behavior in the shell of a mobile modern cephalopod and creates a framework for determining behavior through the analysis of stable isotopes in the extinct ammonites and historically collected *Nautilus*. This work will allow the interpretation of behavior and water column utilization independently from morphological inference, and may allow us to interpret near-surface temperature stratification.

## Materials and Methods

### Ethics statement

The specimen of *Nautilus macromphalus* (Mollusca: Cephalopoda) used in this study was live captured in a baited trap by Dr. Royal H. Mapes in 2002 before the species was given locally

protected status around New Caledonia in 2008. The individual was euthanized and kept for a morphological study of *Nautilus macromphalus*. The sample has been deposited at the American Museum of Natural History (AMNH 105621). The SIMS mount from this sample is housed in the University of Wisconsin Geology museum with the number UW 2009 / 1.2. The *Nautilus belauensis* was hatched from an egg laid in captivity at the Waikiki aquarium as part of the first group of *Nautilus* hatched in captivity in 1990 [45]; however, the individual died for unknown reasons within a month of hatching. The sample is now housed at the American Museum of Natural History (AMNH 102555).

## Sample Material

The wild-caught *Nautilus macromphalus* (AMNH 105621) was live captured in July, 2002 ~20 km south of Nouméa, New Caledonia (Amédée Lighthouse, New Caledonia 22°29'S, 166°27'E, Fig 2). The viscera were removed and the shell was stored dry (Royal H. Mapes pers. comm.). Water temperature near New Caledonia varies with depth (Fig 2) [15]. Temperatures at and near the surface (< 50 m), exhibit a seasonal range. The annual range in surface temperatures spans from 26.3°C to 22.5°C. Temperatures deeper in the water column (<50 m) exhibit minimal (<1°C) temperature seasonality (Fig 2) [15]. The difference between average annual surface water temperature and average annual temperature at 800 m depth is 17.5°C. Surface water  $\delta^{18}\text{O}$  values ( $\delta^{18}\text{O}_{\text{SW}}$ ) of  $0.53 \pm 0.06$  ‰ VSMOW (n = 4 from September to December 1999) were previously reported near the collection site [46] (Fig 2). There are no published seasonal data for  $\delta^{18}\text{O}_{\text{SW}}$  with depth off the coast of New Caledonia, but a seasonal range of 0.16‰ has been predicted from salinity [46]. These data suggest that within the wild-caught *Nautilus macromphalus*,  $\delta^{18}\text{O}_{\text{Arg}}$  variation should record vertical movement during depth migration behavior.

The *Nautilus belauensis* (AMNH 102555) was grown in an 80-liter all-glass aquarium. The aquarium temperature ( $22^\circ\text{C} \pm 1^\circ\text{C}$ ) and one oxygen isotope analysis of the aquarium water (-0.2‰ VSMOW) were reported by Landman et al. [12]. About once a week the water lost due to evaporation (~10%) and remaining water were replaced over an 8-hour period [45,47]. These data about aquarium conditions suggest that variation of  $\delta^{18}\text{O}_{\text{Arg}}$  within the aquarium-reared sample could be the result of changes in  $\delta^{18}\text{O}_{\text{water}}$  due to evaporation from the tank.

The study of the stable isotope geochemistry of *Nautilus* has a long history [5]. Evidence for oxygen isotope equilibrium precipitation of aragonite has been observed for both wild [1–4,6,11,48,49] and for aquarium-reared specimens [12]. Although none of the studies to date have grown *Nautilus* in water with continuous measurement of both  $\delta^{18}\text{O}$  and temperature, it is reasonable to assume that aragonite is precipitated in, or close to, oxygen isotope equilibrium with seawater at ambient temperature given similarity in measurements from field and aquarium data [1,4–8,12]. The calibration of Kim et al. [50] will be used for the equilibrium fractionation of aragonite and water because it was calibrated over a broad temperature range (0–40°C). This calibration also falls within statistical error of the commonly-used formula derived by Grossman and Ku [51]. The Kim et al. [50] equation is as follows:

$$1000 \ln a(^{18}\text{O})_{\text{aragonite-water}} = 17.88 \pm 0.13 \left( \frac{10^3}{T} \right) - 31.14 \pm 0.46 \quad (1)$$

where temperature (T) is in K. Aragonite  $\delta^{18}\text{O}$  values are reported vs. VPDB. Seawater  $\delta^{18}\text{O}$  is reported vs. VSMOW. The  $\delta^{18}\text{O}$  values of seawater and shell aragonite must be reported relative to the same standard to estimate temperature using Eq 1. The conversion between VPDB and VSMOW after Coplen [52], is:

$$\delta^{18}\text{O}_{\text{VSMOW}} = 1.03091 * \delta^{18}\text{O}_{\text{VPDB}} + 30.91 \quad (2)$$

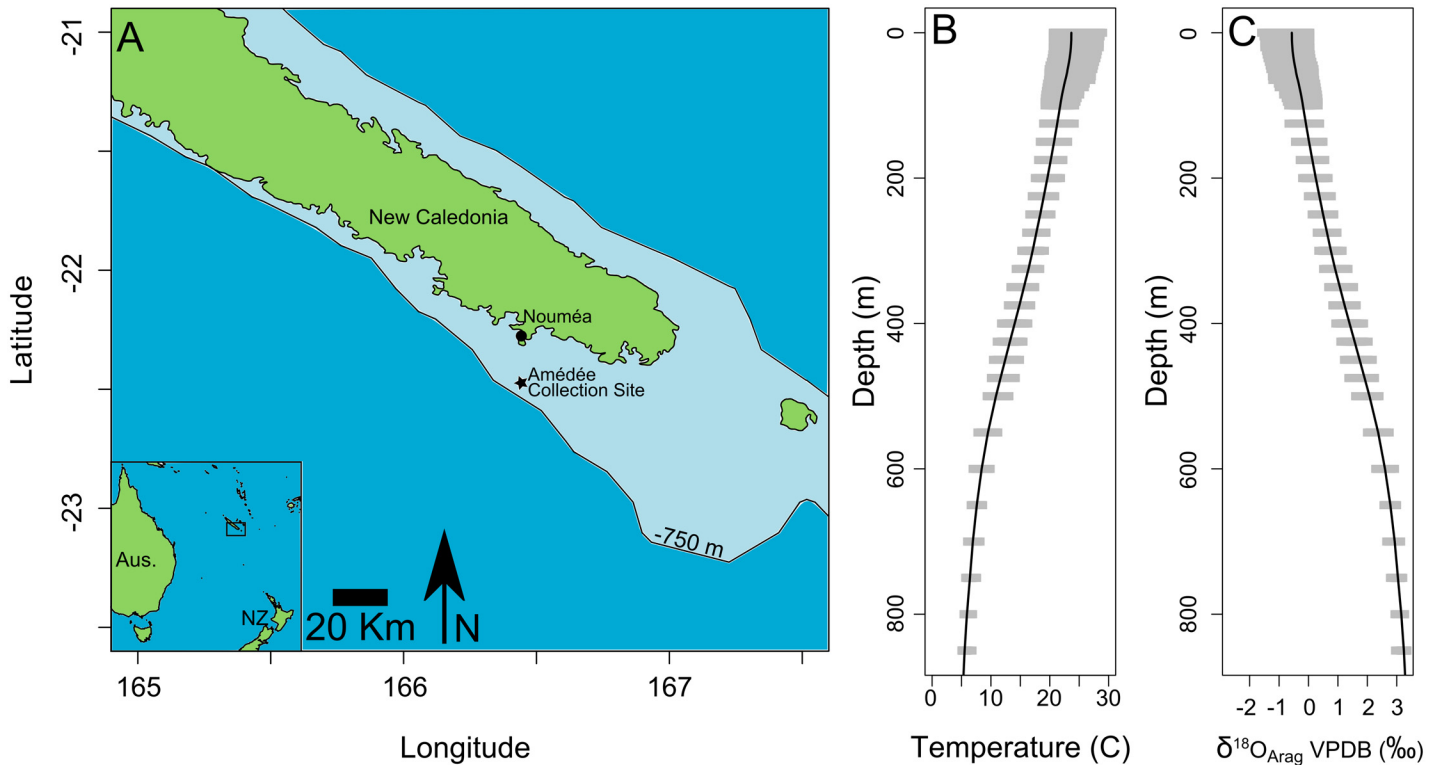


**Fig 2. Map of the collection location of *Nautilus macromphalus* (AMNH 105621) near New Caledonia with  $\delta^{18}\text{O}_{\text{Arag}}$  predicted for the temperatures observed in the water depths *Nautilus* inhabits.** A) Map of the southern end of New Caledonia showing the collection site (Amédée) of the *Nautilus macromphalus* used in this study. The 750 m bathymetry is the approximate lower limit of *Nautilus* habitat in the area defined by implosion depth. B) Water temperature for the map area [15] varies between the surface to 840 m depth. Gray bars indicate the approximate seasonal range in temperatures in the map area at each depth. The black line shows the average annual temperature with depth. A higher amount of seasonal variability is present in the upper 100 meters. C) The expected oxygen isotope ratio calculated using Eq 1 for an aragonite precipitated in isotope equilibrium with seawater at the temperatures shown in B assuming a constant  $\delta^{18}\text{O}_{\text{SW}}$  (0.5‰ VSMOW) with depth. The  $\delta^{18}\text{O}_{\text{Arag}}$  will vary by up to 4‰ over the range of 20°C for the depths that *Nautilus* can inhabit. The gray bars show expected seasonal variability in  $\delta^{18}\text{O}_{\text{Arag}}$  and the black line is the average expected  $\delta^{18}\text{O}_{\text{Arag}}$  with depth in the map area.

doi:10.1371/journal.pone.0153890.g002

where  $\delta^{18}\text{O}_{\text{VSMOW}}$  is the oxygen isotope value reported relative to the Vienna Standard Mean Ocean Water (VSMOW) and  $\delta^{18}\text{O}_{\text{VPDB}}$  is the oxygen isotope value reported relative to the Vienna PeeDee Belemnite (VPDB).

### Preparation of SIMS mounts

SIMS sample mounts of both shells were created from chips removed from sections near the medial plane and near the aperture to maximize the width of the growth bands and growth rate [53]. The analyzed section from the wild-caught *Nautilus macromphalus* was sampled ~3.5 cm from the growth edge, and represents growth in ~December 2001, assuming constant ~182  $\mu\text{m}/\text{day}$  growth. The section from aquarium-reared *Nautilus belauensis* was removed from post-hatching growth. Both shells were roasted separately at 320°C for one hour under vacuum to remove volatile organic matter (after [54,55]). The roasted samples were cast in the center of two, 2.5 cm-diameter epoxy mounts with two grains of UWC-3 calcite standard ( $\delta^{18}\text{O} = 12.49$  ‰, VSMOW; [56]). The surfaces to be analyzed were placed within 5 mm of the center of the mount to minimize instrumental bias of SIMS data caused by sample position [57]. Sample relief was minimized ( $\leq 1$   $\mu\text{m}$ ) to avoid topographic effects on measured  $\delta^{18}\text{O}$  [57]. Initial sectioning of the wild-caught sample through the medial plane (Fig 1) was done with a bandsaw. Growth banding was difficult to image in confocal laser fluorescent

microscopy (CLFM) from surfaces cut by the bandsaw even after epoxy mounting and polishing. The saw removed ~2 mm of the center of the shell and damaged adjacent surfaces making banding difficult to image. Polishing of these surfaces removed less than 50  $\mu\text{m}$  of material. The best sample surfaces for imaging and SIMS analysis did not come from the initial surface cut by the bandsaw, but were produced from shell material that was completely encased in epoxy before being cut with a Buehler Isomet<sup>®</sup> low speed, water cooled saw and that was subsequently polished and finished on a vibrating polisher with a colloidal alumina polish (0.05  $\mu\text{m}$ ).

## Sample Imaging

The polished *Nautilus* shell surfaces were investigated by several techniques to preselect locations for SIMS analysis pits relative to growth banding, determine carbonate mineralogy (calcite vs. aragonite), and to avoid sampling on surface features such as cavities or cracks [58]. Initial analysis was done by scanning electron microscopy (SEM) at UW-Madison, Dept. of Geoscience, utilizing secondary electron (SE) (Fig 3A), cathodoluminescence (CL), backscattered electron (BSE), and electron backscatter diffraction (EBSD) detectors. SE images were used to avoid cracks and cavities. EBSD indicated that the shell material was aragonite and had not changed to calcite during roasting [59]. Growth banding was not clearly resolved by SEM and was imaged in more detail by three other techniques: (1) Confocal laser fluorescent microscopy (CLFM) (Fig 3B), (2) long wavelength (~350 nm) Ultraviolet microscopy (UV) (Fig 3C), and (3) a dissecting microscope (Fig 3D).

## Image Analysis

Images in this study were important in two ways: 1) to guide the placement of SIMS analysis locations by showing the orientation of growth banding and locations of cavities and 2) to provide information on the location of SIMS pits relative to growth banding, which can serve as a chronometer. Images for the wild-caught *Nautilus macromphalus* and aquarium-reared *Nautilus belauensis* are shown in S1 and S2 Figs, respectively. SEM images were specifically used to determine the best placement of SIMS analysis pits to avoid cavities, and CLFM images were used to guide the placement relative to growth banding in order to sample as much growth as possible with sufficient density. ImageJ (version 1.43u [60]) was used to measure the intensity of fluorescence from the monochrome green-black CLFM-image, with values ranging from 255 (Bright green) to 0 (black). Lines 1000 pixels (9 pixels/ $\mu\text{m}$ ) long and one pixel wide parallel to growth banding were averaged by ImageJ to minimize the influence of local variation in luminescence (Fig 1A and 1B). A unified linear reference frame (i.e. distance along a straight line) perpendicular to banding was created by correlating images along growth bands. Multiple CLFM images were required to construct the composite record (S2 Fig). Image-to-image and across-image variation in luminosity was removed by subtracting a lowess regression (to smooth data) through the dataset, leaving the residual variation in luminosity from individual growth bands [61,62]. CLFM luminosity values were matched to the center of SIMS  $\delta^{18}\text{O}_{\text{Arg}}$  pits by equal distance along the axis perpendicular to growth banding.

## SIMS analysis of oxygen isotope ratios

Oxygen isotope ratios were analyzed by SIMS at the WiscSIMS Laboratory, Dept. of Geoscience, UW-Madison, using a CAMECA ims-1280 large-radius multicollector secondary ion mass spectrometer (SIMS). Instrumental conditions were similar to those described by Orland et al. [63] and Kita et al. [57]. A ~1.3 nA primary beam of  $^{133}\text{Cs}^+$  was focused to spots of ~10  $\mu\text{m}$  diameter on the sample surface. Two Faraday Cup detectors were used to simultaneously collect

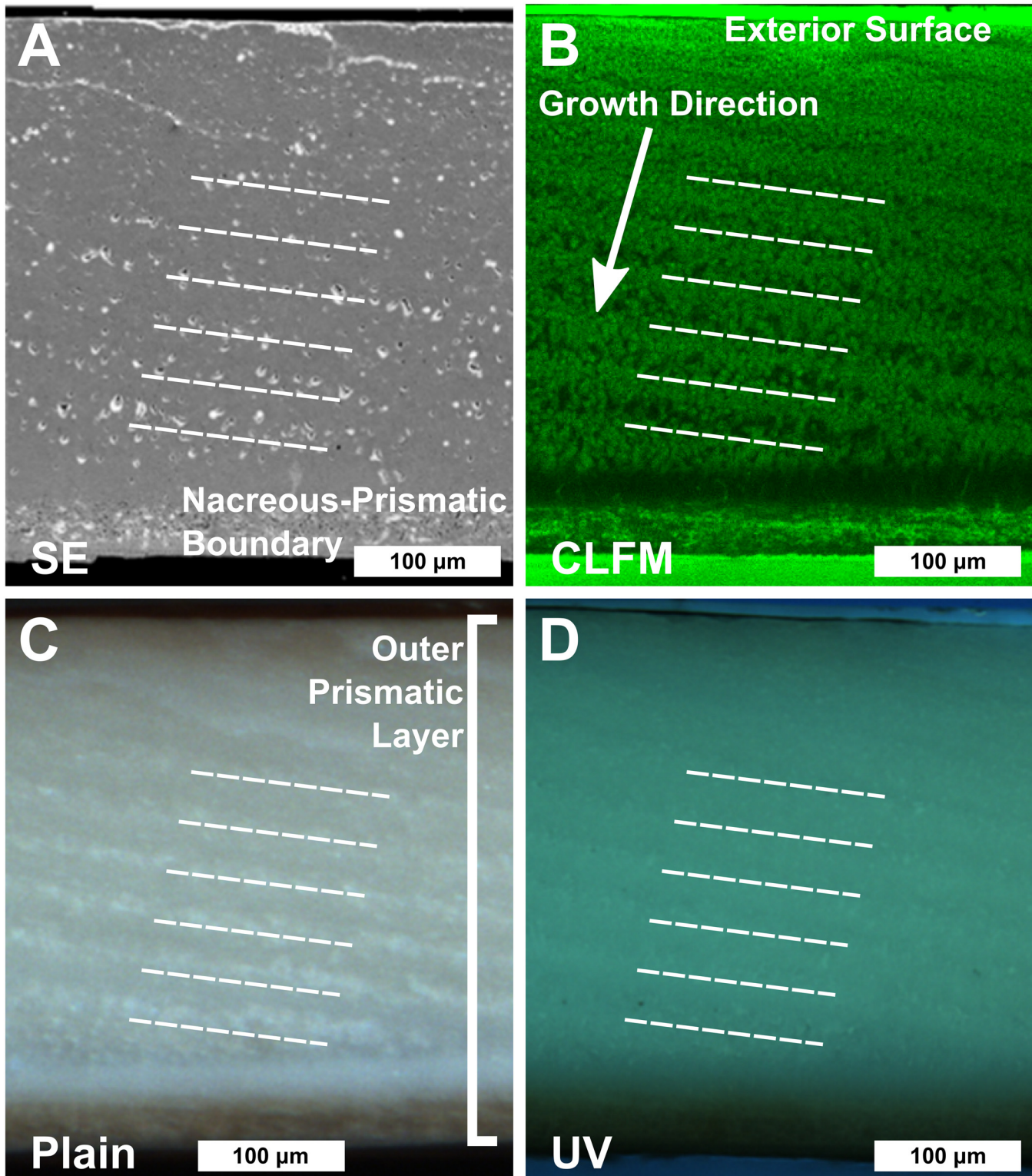


**Fig 3. The outer prismatic layer of a portion of the polished surface from *Nautilus macromphalus* (AMNH 105621) imaged by four different techniques: A) SE, B) CLFM, C) Plain light dissecting microscope, D) UV.** The oldest shell precipitated is in the upper right corner of all images. Growth proceeds to the lower left. All images are of the same portion of the shell. Five bands are highlighted with white lines. A) SE image showing the polished shell surface. Lines of pores in the SE image (A) correlate to low fluorescence in CLFM (B), bright portions of the band in the plain light correlate to dissecting microscope image (C) and dark portions in the long wavelength UV (~360 nm) fluorescence image (D). These cavities are the same as those intersected by

some SIMS analysis pits (Fig 4). B) CLFM (true color) image showing growth bands. Growth bands extend from the exterior surface of the outer prismatic layer (top of the image) to the interior boundary with the nacreous layer. Note that the banding closer to the nacreous boundary is more pronounced than the banding toward the exterior of the shell. C) Plain-light dissecting microscope image (true color) of polished shell surface. Banding is apparent but discontinuous. D) UV fluorescence (true color) image of the shell. Faint banding is present with an orientation equal to that found in other imaging techniques. CLFM images on the uncoated sample mount were made using a Bio-Rad MRC-1024 scanning confocal microscope at the W. M. Keck Laboratory for Biological Imaging at UW-Madison operated with a 40 mW laser at a wavelength of 488 nm. Images of banding within the outer prismatic layer were best expressed through an emission filter that detects visible green light ( $\lambda = 505$  to 539 nm). Growth-band orientation in the prismatic layer was used to place SIMS transects.

doi:10.1371/journal.pone.0153890.g003

$^{18}\text{O}^-$  and  $^{16}\text{O}^-$  ions during all sessions. In 2013 and 2014, one additional Faraday Cup was used to collect  $^{16}\text{O}^1\text{H}^-$  ions. Pits were sputtered to a depth of  $\sim 1$   $\mu\text{m}$ . Surface charging was compensated by an electron flood gun in combination with a  $\sim 20$  nm thick carbon coat (*Nautilus macromphalus* in 2011) or gold coat (*Nautilus macromphalus* in 2014, *Nautilus belauensis* in 2013) which was applied after final polishing and surficial cleaning. Surficial cleaning with deionized water and ethanol was brief to minimize risk of surface etching.

A total of 571 SIMS analyses of  $\delta^{18}\text{O}$  were made: 193 on standards, 295 analyses on the wild-caught sample and 84 analyses on the aquarium-reared sample. Analyses on the wild-caught sample were performed over two sessions, 6/28/2011–6/29/2011 and 2/14/2014–2/15/2014. Analyses on the aquarium-reared sample were conducted on 9/25/2013 and 9/26/2013. Groups of 10–15 sample analyses were bracketed by four analyses before and four analyses after of UWC-3 calcite standard. The precision of the eight bracketing standard analyses was used to define the spot-to-spot precision of sample analyses [64] that averaged  $\pm 0.3\%$  ( $\pm 2$  SD) for this dataset. The UWC-3 calcite standard [56] was used as a running standard for aragonite. A difference in instrumental bias (sometimes called Instrumental Mass Fractionation) between the two polymorphs has been observed [59,65]. The UW Arg-7 aragonite standard was compared to the UWC-3 calcite standard ( $\delta^{18}\text{O} = 12.49$  ‰, VSMOW; [56]) on 9/25/2013 when the aquarium-reared sample was analyzed and the wild-caught sample was analyzed on 2/14/2014. We recalibrated the UW Arg-7 standard to  $\delta^{18}\text{O} = 19.73$  ‰ (VSMOW) from  $\delta^{18}\text{O} = 20.03$  ‰ (VSMOW) as reported by Orland [65]. Orland [65] calibrated this standard from analyses at the University of Wisconsin-Madison using the phosphoric acid fractionation factor for aragonite at 25°C ( $\alpha_{\text{CO}_2(\text{Acid-Aragonite})} = 1.01034$ ) reported by Freidman and O'Neil [66]. Here we use the phosphoric acid fractionation factor from Kim et al. [67] at 25°C ( $\alpha_{\text{CO}_2(\text{Acid-Aragonite})} = 1.01063$ ) to recalibrate the value because Kim et al. [67] dataset was large ( $n = 29$  for aragonite) and therefore reduced statistical uncertainty by a factor of 3.8 over the value reported by Freidman and O'Neil [66]. The difference in SIMS instrumental bias between aragonite and calcite was 0.61‰ for the session when the aquarium reared sample was analyzed, and 0.57‰ when the wild-caught sample was analyzed. The difference in bias between calcite and aragonite (0.81‰) for data collected in 2011 [68] was estimated by comparing the mean  $\delta^{18}\text{O}_{\text{Arg}}$  values of populations (6/28/2011–6/29/2011 vs. 2/14/2014–2/15/2014) of very closely spaced analyses on the shell.

## Evaluation of the SIMS analysis pits in *Nautilus* shell

SIMS analysis pits were imaged by SEM to screen for irregular pit shapes before interpretation of the data (Fig 4, S1 and S2 Figs) [58]. Data from SIMS pits that intersect cavities, cracks, or inclusions are not guaranteed to be reliable [56,69,70]. Cracks were readily avoided during analysis; however, the roasting procedure appears to have removed intercrystalline organic matter, leaving small cavities that were difficult to avoid. Five pits are displayed that are representative examples for the range of pit-cavity interaction and these were used as a guide for the classification of the remaining pits (Fig 4). Pit categories were based on inspection of SEM images only and not on measured  $\delta^{18}\text{O}_{\text{Arg}}$ . Pits designated category 1 (C1) have no cavity intersection visible



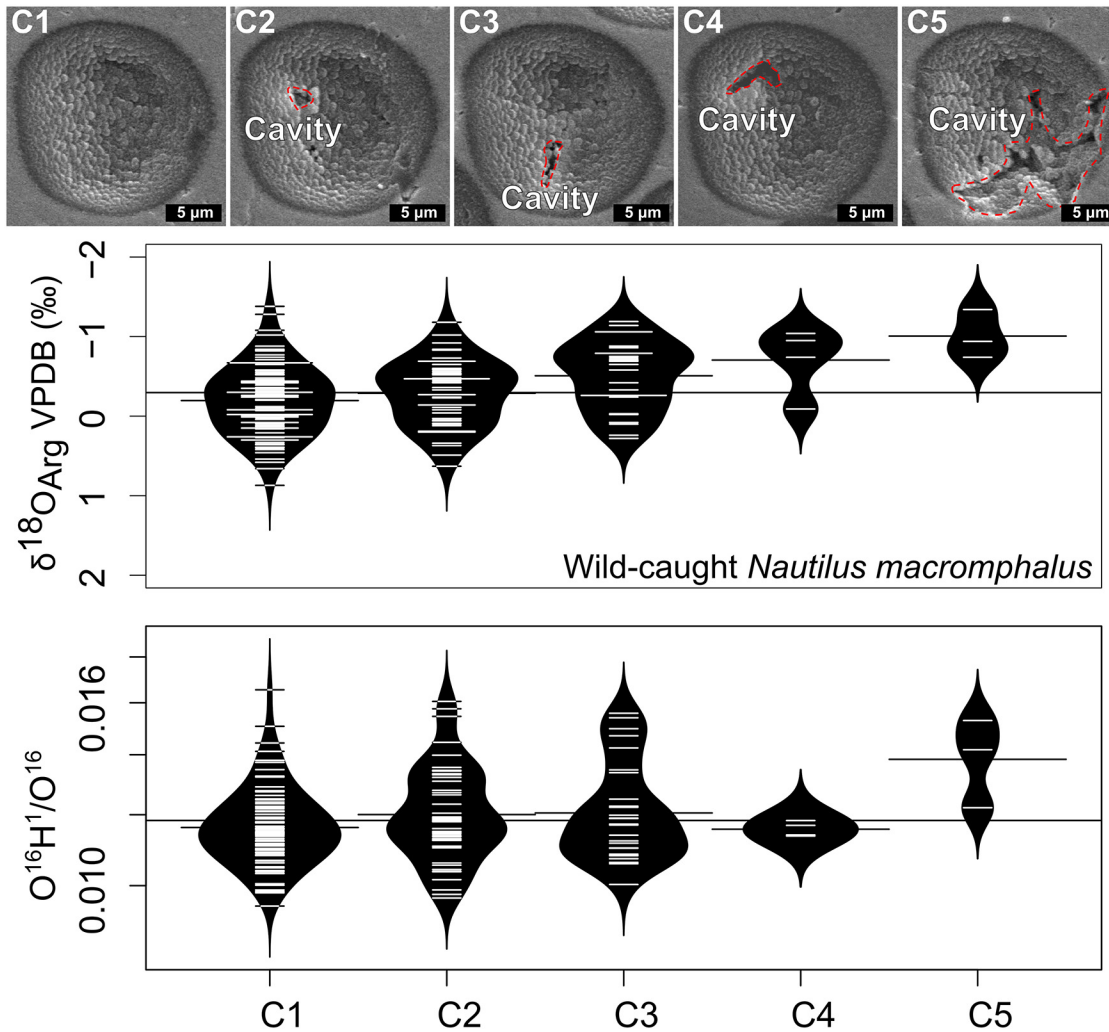


**Fig 4. Representative SE images illustrating the criteria used for qualitative SIMS pit categorization for both the wild-caught and aquarium-reared *Nautilus* and beanplots showing the distribution of  $\delta^{18}\text{O}_{\text{Arg}}$  and  $\text{O}^{16}\text{H}^1/\text{O}^{16}$  across pit categories from *Nautilus macromphalus* (AMNH 105621).** Cavities that the SIMS analysis pits intersected are likely left from the removal of organic matter during roasting or from plucking during polishing. Organic matter in the outer prismatic layer of mollusks has banding but also irregular clumps [22]. In the images above, cavities are outlined by a red dashed line. All pits are approximately 1- $\mu\text{m}$  deep. Category 1 (C1) This pit is classified as regular in appearance because it has a uniform texture throughout the walls and bottom of the pit (wild-caught,  $n = 134$ ; aquarium-reared,  $n = 25$ ). Category 2 (C2) This pit minimally intersects two small cavities and therefore is also classified as regular in appearance (wild-caught,  $n = 85$ ; aquarium-reared,  $n = 5$ ). Category 3 (C3) A more significant intersection with a cavity at the bottom of this analysis pit makes it irregular (wild-caught,  $n = 52$ ; aquarium-reared,  $n = 16$ ). Category 4 (C4) A larger intersection with a cavity, but this cavity intersection is on the wall of the pit rather than on the bottom. This pit is also considered to be irregular and 5% of analyses had cavity intersections similar to this pit (wild-caught,  $n = 14$ ; aquarium-reared,  $n = 7$ ). Category 5 (C5) This pit is an example of some of the most extreme pit-cavity intersections and is a highly irregular pit (wild-caught,  $n = 8$ ; aquarium-reared,  $n = 0$ ). Beanplots [71] below show the estimated density distribution of  $\delta^{18}\text{O}_{\text{Arg}}$  (top) or  $\text{O}^{16}\text{H}^1/\text{O}^{16}$  (bottom) for the wild-caught *Nautilus macromphalus* where we have paired analyses (2/14/2014-2/15/2014). The thin black line extending across the beanplots indicates the mean for all analyses, short lines extending from each category indicate each category mean, and short white lines within each category indicate individual observations.

doi:10.1371/journal.pone.0153890.g004

by SEM. Pits designated category 2 (C2) intersect small cavities ( $< 1 \mu\text{m}$ ) on the edge of the pit. Category 3 (C3) pits intersect slightly larger cavities ( $\sim 1 \mu\text{m}$ ) in the bottom or sides of the pit. Pits in category 4 (C4) intersect cavities that are 2–3  $\mu\text{m}$  wide. Pits designated category 5 (C5) intersect cavities in the shell larger than 3  $\mu\text{m}$ . An additional filter of  $>95\%$  yield relative to the bracketing UWC-3 calcite data was also applied to data from both the wild-caught and aquarium-reared samples to screen for irreproducible  $\delta^{18}\text{O}_{\text{Arg}}$  measurements [58].

## Results

### Growth banding

Banding within the outer prismatic layer is apparent in CLFM, plain light on a binocular microscope, and UV light fluorescence microscopy (Fig 3). The banding intersects the exterior surface of the shell and the nacreous-prismatic boundary at low angles ( $\sim 11^\circ$ ). A single band is defined by the change in fluorescence from low to high and back to low again (Figs 1 and 3B). The number and distribution of bands observed in the outer prismatic layer is equal for all of the imaging techniques, but clarity of banding differs between imaging techniques. Banding is not readily discernible in SEM (Fig 3A), but there are concentrations of cavities that have the same orientation and spacing as banding visible under other imaging techniques. Cavities are defined as holes in the shell carbonate visible in SE images (black spots with white rims, from charging in Fig 3A). Bands of cavities correlate with low fluorescence in CLFM, the dark portion of bands in UV and the bright portion of the bands in plain light. CLFM produced images of banding that are the clearest out of any technique (Fig 3B). The banding is also apparent in plain light, but some bands are not very pronounced (Fig 3C). Banding is also discernible in long-wavelength ( $\sim 360$  nm) UV (Fig 3D), but the delineation of band edges was less pronounced in unadjusted (contrast—brightness unenhanced) images than in plain light. The visibility of banding dramatically improved over bandsaw cut edges when shell was cut by a Buehler Isomet<sup>®</sup> low speed diamond saw and subsequently polished and finished with a colloidal alumina polish ( $0.05\ \mu\text{m}$ ).

The intraprismatic growth banding of the wild-caught sample of *Nautilus macromphalus* is readily visible in CLFM images. The contrast between low fluorescence and high fluorescence portion of each band varies between the end of the band near the prismatic-nacreous boundary (Fig 1, Box B) and the exterior surface of the shell (Fig 1, Box A). The contrast between low fluorescence and high fluorescence portions of bands is greater near the prismatic-nacreous boundary and lower toward the exterior shell surface. The apparent ‘graininess’ of bands, i.e. the size of shapes with uniform or nearly uniform fluorescence, also varies along the expression of a single band. Graininess is low toward the exterior of the shell and increases toward the prismatic-nacreous boundary.

**Apertural growth rate estimated by CLFM Imaging.** The thickness of well-expressed bands in CLFM averages  $34.7\ \mu\text{m}$  (measured normal to bands) across the sampled portion of the wild-caught *Nautilus macromphalus* with a standard deviation of  $8.6\ \mu\text{m}$  and a range from  $19.8$  to  $58.9\ \mu\text{m}$ . Growth band thickness can be compared to published apertural growth rates if width is converted to distance in the apertural direction. An average apertural growth of  $182\ \mu\text{m}$  per band is obtained using the angle of banding intersection ( $\sim 11^\circ$ ) and band width ( $34.7\ \mu\text{m}$ ) (Fig 1). Apertural growth per band in the wild-caught *Nautilus macromphalus* is between  $104$  and  $308\ \mu\text{m}$ . In the aquarium-reared sample, growth banding in CLFM averages  $20.1\ \mu\text{m}$  (measured normal to banding) across 14 bands with a standard deviation of  $6.1\ \mu\text{m}$  and a range of  $12.4$  to  $30.7\ \mu\text{m}$ . This translates to a growth rate of  $105\ \mu\text{m}/\text{day}$  and a range from  $65$  to  $160\ \mu\text{m}/\text{day}$  assuming banding is daily. Growth rates reported in literature span from  $80$  to  $300\ \mu\text{m}$  per day and nearly encompass the entire range of values calculated from growth band width in these two individuals [21,42,72–74].

### Oxygen Isotope Ratios

**Evaluation of SIMS pit appearance as criteria for acceptance or rejection of data.** Analysis pit locations were selected carefully using the reflected light optics of the IMS-1280 during analysis and correlating with images made of porosity before analysis. However,  $2\text{-}\mu\text{m}$ -scale

features are difficult to see [75] in the coated sample surface and 74 (25%) of the 295 analyses on the wild-caught sample intersected cavities that were identified by SEM after analysis. Perhaps due to higher cavity density or more evenly distributed small cavities, 23 (43%) of 53 analyses on the aquarium-reared sample intersected subsurface cavities. Five categories were qualitatively defined by the amount of pit intersection and pits were assigned to a category by inspection of SEM images (Fig 4).

A systematic trend of decreasing  $\delta^{18}\text{O}_{\text{Arg}}$  is present with increasing cavity intersection (Fig 4) (ANOVA wild-caught  $p < 0.001$ , aquarium-reared,  $p = 0.014$ ). Mean  $\delta^{18}\text{O}_{\text{Arg}}$  for the five categories, listed in increasing amount of intersection with cavities for the wild-caught sample, are:  $-0.3\text{‰}$  (C1,  $n = 134$ );  $-0.5\text{‰}$  (C2,  $n = 85$ );  $-0.6\text{‰}$  (C3,  $n = 52$ );  $-1.1\text{‰}$  (C4,  $n = 14$ ); and  $-2.3\text{‰}$  (C5,  $n = 8$ ). Mean  $\delta^{18}\text{O}_{\text{Arg}}$  for the aquarium-reared sample pit categories, are  $-1.3\text{‰}$  (C1,  $n = 25$ ),  $-1.5\text{‰}$  (C2,  $n = 5$ ),  $-1.4$  (C3,  $n = 16$ ),  $-1.9$  (C4,  $n = 7$ ), and no points were classified as C5. In the wild-caught *Nautilus macromphalus*, the mean  $\delta^{18}\text{O}_{\text{Arg}}$  of pits with the most cavity intersection (C5) is  $2\text{‰}$  lower than that of the group with the least cavity intersection (C1). In the aquarium-reared *Nautilus belauensis*, the mean  $\delta^{18}\text{O}_{\text{Arg}}$  of pits with the most cavity intersection (C4) is  $\sim 0.5\text{‰}$  lower than that of the group with the least cavity intersection (C1). Analyses from irregular pits (C3, C4, C5) may not accurately measure the  $\delta^{18}\text{O}$  of aragonite. Although cavities appear to correlate to areas with lower CLFM luminosity (Fig 3), irregular pits are not grouped in areas with high or low CLFM brightness (ANOVA wild-caught  $p = 0.12$ ; aquarium-reared  $p = 0.13$ ). The two categories of pits with minimal cavity intersection (C1 and C2, aquarium-reared sample  $n = 30$ , Table 1, wild-caught sample  $n = 219$ , Table 2) are considered regular and will be discussed further. Exclusion of pits in categories C3, C4 and C5 (Fig 3) does not significantly alter the interpretation of this dataset for either wild-caught or aquarium reared specimens and inclusion of these would only increase the variation observed in  $\delta^{18}\text{O}_{\text{Arg}}$ , especially within the wild-caught specimen. The complete dataset for the wild-caught *Nautilus macromphalus* (AMNH 105621) is in S1 Table and the complete dataset for the aquarium-reared *Nautilus belauensis* (AMNH 102555) is in S2 Table.

**$\delta^{18}\text{O}$  variation and CLFM fluorescence.** SIMS oxygen isotope analysis of the prismatic layer of both samples shows no correlation between measured oxygen isotope ratios and CLFM fluorescence at pit locations. For the wild-caught sample, both Pearson's product-moment correlation ( $p = 0.17$ ,  $\text{cor} = 0.15$ ) for all regular pits (C1 and C2) and Spearman's rank order correlation ( $p = 0.24$ ,  $\rho = 0.13$ ) are of low magnitude and not statistically significant. Likewise, for the aquarium-reared sample, both correlation tests are of low magnitude and non-significant (Pearson  $\text{cor} = 0.11$ ,  $p = .58$  and Spearman  $\rho = 0.047$ ,  $p = .844$ ).

**$\delta^{18}\text{O}$  variation within bands.** SIMS oxygen analyses vary within the bands visible in CLFM images (Figs 5 and 6). The amount of variation captured by analysis is dependent on the pit spacing within the band and the placement of the pits. Bands with more pits (3 or more) are more likely to have a large range in  $\delta^{18}\text{O}_{\text{Arg}}$ . In the wild-caught sample, variation beyond instrument precision (2SD) is observed in 26 of the 39 bands that contain 2 or more analysis pits with an average within band range in  $\delta^{18}\text{O}_{\text{Arg}}$  of  $0.8\text{‰}$  and a maximum range of  $1.5\text{‰}$  (Fig 5). Within the aquarium-reared sample, only 2 of the 4 bands with three or more pits had ranges outside of expectations for instrumental precision with an average range of  $0.6\text{‰}$  and a maximum range of  $1\text{‰}$  (Fig 6). Correlation between transect locations shows nearly equal  $\delta^{18}\text{O}$  values between closely spaced pits on the traverse perpendicular to banding (Figs 5 and 6).

**$\delta^{18}\text{O}$  variation across bands.** Cycles are present across several bands in both the wild-caught sample and the aquarium-reared sample (Figs 5 and 6). The wild-caught sample has several cycles that occur across 2–3 bands. The aquarium-reared sample has one long-term

**Table 1. Summary of SIMS analyses of oxygen isotope ratios measured at WiscSIMS on the *Nautilus belauensis* (AMNH 102555) and confocal microscope brightness.** These are ion microprobe analyses of oxygen isotope ratios, grey scale values from confocal laser fluorescence images, and distance perpendicular to banding for analyses that were shown to be regular based on pit morphology. See supplementary material for a complete list of measurements.

Analysis Name	$\delta^{18}\text{O}_{\text{VPDB}}^{**}$ (‰)	$\delta^{18}\text{O}_{\text{VSMOW}}^*$ (‰)	Error <sup>£</sup> (2s.d.)	$\delta^{18}\text{O}_{\text{Raw}}^{\wedge}$ (‰)	Relative Yield <sup>€</sup> (%)	Pit category <sup>Ω</sup>	Dist. <sup>κ</sup> (μm)	CLFM Greyscale <sup>^</sup>
2-9	-1.7	29.2	0.3	27.1	97.60	1	8.1	0.40
2-6	-1.0	29.9	0.3	27.8	95.00	1	49.4	2.81
2-5	-1.7	29.2	0.3	27.2	95.70	2	54.2	-0.81
3-12	-1.4	29.5	0.4	27.4	96.60	1	60.5	-4.19
3-10	-0.8	30.1	0.4	28.0	96.30	1	65.3	-4.52
2-4	-0.8	30.1	0.3	28.1	95.30	1	66.1	-4.31
3-9	-0.8	30.1	0.4	28.0	95.80	1	69.2	-0.20
3-8	-0.7	30.2	0.4	28.1	96.10	1	78.8	9.39
3-7	-1.0	29.9	0.4	27.8	95.50	2	87.5	-6.69
3-6	-0.9	30.0	0.3	27.9	96.70	1	99.4	0.98
3-5	-0.8	30.1	0.3	28.0	95.60	1	107.3	-2.84
3-13	-1.6	29.3	0.4	27.2	96.20	1	108.1	-1.81
1-10	-1.1	29.8	0.4	27.8	96.60	1	116.9	1.12
1-9	-1.6	29.3	0.4	27.3	97.80	1	125.6	-3.90
3-3	-1.4	29.5	0.3	27.4	96.20	1	132.7	1.13
1-8	-1.4	29.5	0.4	27.5	97.80	1	134.3	0.75
3-2	-1.5	29.3	0.3	27.2	95.70	1	139.9	2.48
1-7	-1.5	29.4	0.4	27.4	97.50	1	143.0	8.08
3-1	-1.8	29.1	0.3	27.0	95.90	1	148.6	-7.16
1-4	-1.8	29.1	0.4	27.1	96.90	1	174.0	0.84
1-3	-1.8	29.1	0.4	27.1	97.30	2	189.9	-1.39
4-14	-1.9	29.0	0.2	27.1	98.30	1	208.9	-3.36
4-8	-1.9	29.0	0.3	27.1	98.10	1	216.9	0.66
4-18	-1.1	29.8	0.2	27.9	95.40	1	228.8	1.66
4-7	-2.2	28.7	0.3	26.8	98.70	1	232.7	0.06
4-12	-1.6	29.3	0.2	27.4	97.00	2	236.7	-2.80
4-5	-1.5	29.4	0.3	27.5	97.60	2	258.9	-6.19
4-3	-1.4	29.5	0.3	27.6	97.80	1	280.3	-0.98

Analysis names refer to Transect#-Pit#.

\*\* Conversion from VSMOW and corrected to aragonite  $\delta^{18}\text{O}_{\text{VPDB}} = (\delta^{18}\text{O}_{\text{VSMOW}} - 30.91)/1.03091$ .

\* Value adjusted by bracketing UWC-3 calcite standard and corrected to aragonite (-0.61‰), see text.

<sup>^</sup> Value reported vs. VSMOW  $\delta^{18}\text{O}_{\text{Raw}} = \{({}^{18}\text{O}/{}^{16}\text{O} \text{ measured}/0.00200520) - 1\} * 1000$

<sup>£</sup> Precision for  $\delta^{18}\text{O}_{\text{VPDB}}$  measurements derived from 2 times standard deviation of eight bracketing standards.

<sup>€</sup> Yield (counts per second/nA, a measure of ionization efficiency) relative to the mean yield of 8 bracketing standards for UWC-3 calcite.

<sup>Ω</sup> Pit category defined by SEM images compared to images in Fig 4.

<sup>κ</sup> Distance values in micrometers perpendicular to visible banding to center of analysis pit.

<sup>^</sup> Normalized CLFM grey scale value from averaged line of pixels parallel to growth banding in CLFM image for pit location with lowess regression removed to correct for trends in brightness across and between images. Low values are dark portions of growth bands and high values are bright portion.

doi:10.1371/journal.pone.0153890.t001

cycle across 8 bands where an increase in  $\delta^{18}\text{O}$  is slow over 5 bands, and then there is a rapid decrease over 3 bands (from 275–50 h, Fig 6). The range of  $\delta^{18}\text{O}_{\text{Arg}}$  measured in the wild-caught sample was from 0.6 to -1.9‰ (VPDB). In the aquarium-reared sample the range was 1‰ smaller than that of the wild-caught sample (measured values from -1 to -2.5‰ VPDB).

**Table 2. Summary of SIMS analyses of oxygen isotope ratios measured at WiscSIMS on the *Nautilus macromphalus* (AMNH 105621) and confocal microscope brightness.** These are ion microprobe analyses of oxygen isotope ratios, grey scale values from confocal laser fluorescence images, and distance perpendicular to banding for analyses that were shown to be regular based on pit morphology. See supplementary material for a complete list of measurements.

Analysis Name	$\delta^{18}\text{O}_{\text{VPDB}}^{**}$ (‰)	$\delta^{18}\text{O}_{\text{VSMOW}}^*$ (‰)	Error <sup>c</sup> (2s.d.)	$\delta^{18}\text{O}_{\text{Raw}}^{\wedge}$ (‰)	Date	RelativeYield <sup>e</sup> (%)	Dist. <sup>k</sup> (μm)	Pit quality	CLFM Greyscale <sup>^</sup>
0-1	-0.7	30.2	0.2	26.9	2/14/2014	97.00	23.7	1	1.61
0-2	0.0	31.0	0.2	27.7	2/14/2014	97.00	36.2	1	1.43
0-3	-0.4	30.5	0.2	27.2	2/14/2014	96.70	38.0	1	3.11
1-1	-0.8	30.1	0.2	25.3	6/28/2011	95.36	38.0	1	3.11
1-2	-1.3	29.6	0.2	24.8	6/28/2011	95.31	43.8	2	3.41
0-4	0.3	31.2	0.2	27.9	2/14/2014	96.10	47.9	1	2.62
0-5	0.2	31.1	0.2	27.8	2/14/2014	96.70	77.5	1	3.96
1.5-1	-0.1	30.8	0.5	27.8	2/14/2014	95.30	80.2	1	2.73
1-7	-1.0	29.9	0.2	25.1	6/28/2011	95.29	87.8	1	-3.15
0-6	0.1	31.0	0.2	27.7	2/14/2014	96.70	91.4	2	-4.18
1.5-2	-0.7	30.1	0.5	27.1	2/14/2014	96.40	96.7	1	-2.58
0-7	0.4	31.3	0.2	28.0	2/14/2014	97.00	106.6	1	4.04
0-8	0.0	30.9	0.2	27.7	2/14/2014	96.70	108.9	1	4.29
1.5-3	-0.3	30.6	0.5	27.6	2/14/2014	96.10	112.0	1	2.00
0-9	0.1	31.0	0.2	27.7	2/14/2014	97.60	126.8	1	-1.95
1-11	-1.3	29.6	0.2	24.7	6/28/2011	95.52	126.8	2	-1.95
1.5-5	0.1	31.0	0.5	28.0	2/14/2014	97.90	130.4	2	-0.92
0-10	0.2	31.1	0.2	27.8	2/14/2014	96.90	141.6	2	3.30
0-11	-0.2	30.7	0.5	27.6	2/14/2014	97.10	153.8	2	-1.80
2-15	-0.7	30.2	0.1	25.4	6/29/2011	96.17	166.3	1	-1.55
1-15	-1.4	29.4	0.2	24.6	6/28/2011	95.46	171.2	2	0.64
0-13	-0.7	30.2	0.5	27.2	2/14/2014	97.50	172.5	2	1.78
1.5-7	-0.1	30.8	0.5	27.7	2/14/2014	96.60	173.0	2	1.74
2-3	-0.7	30.2	0.2	25.3	6/28/2011	95.36	177.5	2	0.20
2-2	-0.6	30.2	0.2	25.4	6/28/2011	96.14	179.3	2	0.28

(Continued)

Table 2. (Continued)

Analysis Name	$\delta^{18}\text{O}_{\text{VPDB}}^{**}$ (‰)	$\delta^{18}\text{O}_{\text{VSMOW}}^*$ (‰)	Error <sup>c</sup> (2s.d.)	$\delta^{18}\text{O}_{\text{Raw}}^{\wedge}$ (‰)	Date	RelativeYield <sup>e</sup> (%)	Dist. <sup>k</sup> (µm)	Pit quality	CLFM Greyscale <sup>^</sup>
1–16	-0.4	30.5	0.2	25.7	6/28/2011	95.47	179.7	2	0.24
0–14	0.3	31.3	0.5	28.2	2/14/2014	97.20	184.2	2	-0.70
0–15	-0.1	30.8	0.5	27.8	2/14/2014	97.40	187.3	2	0.22
2–17	-0.8	30.1	0.1	25.3	6/29/2011	96.37	189.1	2	-0.18
1.5–8	-0.6	30.3	0.5	27.3	2/14/2014	97.20	192.3	2	1.67
2–4	-1.1	29.8	0.2	25.0	6/28/2011	95.47	193.2	2	2.13
1.5–9	-0.8	30.1	0.5	27.0	2/14/2014	97.60	201.7	2	0.82
2–18	-0.9	30.0	0.1	25.1	6/29/2011	96.42	202.1	1	0.85
2–19	-0.9	30.0	0.1	25.2	6/29/2011	96.13	213.3	2	2.93
2–6	-0.2	30.7	0.3	25.8	6/28/2011	96.57	220.5	1	-3.48
0–18	-0.5	30.4	0.5	27.4	2/14/2014	97.20	222.3	2	-3.51
2–20	-0.7	30.2	0.1	25.4	6/29/2011	96.69	226.3	1	-4.81
2–21	0.0	30.9	0.1	26.1	6/29/2011	96.21	236.2	1	-0.56
0–20	-0.1	30.8	0.5	27.8	2/14/2014	98.60	238.9	2	-0.13
0–19	0.3	31.2	0.5	28.1	2/14/2014	97.20	242.5	1	2.25
2–8	-0.4	30.5	0.3	25.6	6/28/2011	96.69	245.2	1	1.92
2–9	-1.1	29.7	0.3	24.8	6/28/2011	95.73	257.3	1	0.05
2–23	-0.6	30.3	0.1	25.5	6/29/2011	96.98	260.0	2	-0.99
2–24	-1.2	29.7	0.1	24.9	6/29/2011	97.12	273.0	2	-0.96
2–13	-0.8	30.1	0.3	25.1	6/28/2011	95.99	285.1	1	-0.93
3–2	-0.3	30.6	0.2	25.6	6/29/2011	95.60	320.5	1	-1.91
3–13	-0.2	30.8	0.2	25.9	6/29/2011	96.09	335.8	1	2.91
3–4	-0.4	30.5	0.2	25.5	6/29/2011	96.17	344.7	1	5.99
3–14	-0.3	30.6	0.2	25.8	6/29/2011	96.60	346.5	2	4.45
3–6	-1.0	29.9	0.2	24.9	6/29/2011	96.83	366.3	1	-2.53
3–16	-0.8	30.1	0.2	25.2	6/29/2011	96.99	368.0	2	-0.30

(Continued)

Table 2. (Continued)

Analysis Name	$\delta^{18}\text{O}_{\text{VPDB}}^{**}$ (‰)	$\delta^{18}\text{O}_{\text{VSMOW}}^*$ (‰)	Error <sup>c</sup> (2s.d.)	$\delta^{18}\text{O}_{\text{Raw}}^{\wedge}$ (‰)	Date	RelativeYield <sup>e</sup> (%)	Dist. <sup>k</sup> (µm)	Pit quality	CLFM Greyscale <sup>^</sup>
3-7	-0.2	30.7	0.2	25.7	6/29/2011	96.37	377.9	1	2.72
3-8	0.0	30.9	0.2	25.9	6/29/2011	96.58	382.4	2	0.08
3-17	-0.4	30.5	0.2	25.6	6/29/2011	96.91	382.4	2	0.08
3-18	-0.6	30.3	0.2	25.4	6/29/2011	97.75	392.7	1	-2.86
3-19	-0.2	30.7	0.2	25.9	6/29/2011	97.16	400.3	1	1.16
3-9	-0.2	30.7	0.2	25.7	6/29/2011	95.74	404.8	1	2.48
3-20	-0.8	30.1	0.2	25.3	6/29/2011	96.57	419.2	1	-0.12
3-21	-0.9	30.0	0.2	25.2	6/29/2011	97.09	431.3	1	0.24
3-22	-0.5	30.4	0.2	25.5	6/29/2011	97.00	440.2	1	1.37
3-12	-0.5	30.3	0.2	25.4	6/29/2011	97.75	443.8	2	0.15
4-3	-0.5	30.4	0.2	25.6	6/29/2011	95.24	446.5	1	-0.90
3-23	-1.6	29.3	0.2	24.4	6/29/2011	95.23	449.2	2	-0.62
4-4	-1.2	29.7	0.2	24.9	6/29/2011	97.15	458.2	1	-3.71
3-24	-0.5	30.3	0.2	25.5	6/29/2011	98.01	465.4	1	-2.71
4-5	-0.6	30.3	0.2	25.6	6/29/2011	96.58	473.4	2	-0.11
4-6	-0.5	30.4	0.2	25.7	6/29/2011	96.40	482.8	2	-1.30
4-7	-0.5	30.3	0.2	25.6	6/29/2011	96.20	490.5	1	0.48
4-20	-0.6	30.3	0.2	25.5	6/29/2011	96.87	492.3	2	1.94
4-8	-0.5	30.4	0.2	25.6	6/29/2011	96.79	498.5	1	5.71
4-21	-0.7	30.2	0.2	25.4	6/29/2011	97.02	504.8	2	2.68
4-9	0.1	31.0	0.2	26.2	6/29/2011	96.76	512.4	1	-2.80
4-11	-0.5	30.4	0.2	25.6	6/29/2011	96.31	533.1	1	1.87
4-23	-0.3	30.6	0.2	25.8	6/29/2011	96.29	536.7	1	0.18
4-12	-0.5	30.4	0.2	25.7	6/29/2011	96.25	544.3	2	1.42
4-24	-0.4	30.5	0.2	25.7	6/29/2011	96.06	549.2	2	0.63
4-13	-0.7	30.2	0.1	25.5	6/29/2011	97.28	556.8	1	-1.79

(Continued)

Table 2. (Continued)

Analysis Name	$\delta^{18}\text{O}_{\text{VPDB}}^{**}$ (‰)	$\delta^{18}\text{O}_{\text{VSMOW}}^*$ (‰)	Error <sup>c</sup> (2s.d.)	$\delta^{18}\text{O}_{\text{Raw}}^{\wedge}$ (‰)	Date	RelativeYield <sup>e</sup> (%)	Dist. <sup>k</sup> (µm)	Pit quality	CLFM Greyscale <sup>^</sup>
4-14	-1.0	29.9	0.1	25.2	6/29/2011	96.58	564.5	1	-3.18
5-1	-1.2	29.7	0.1	25.0	6/29/2011	96.26	576.1	1	4.74
4-16	0.0	30.9	0.1	26.1	6/29/2011	96.71	577.5	1	4.52
4-26	-0.2	30.7	0.2	25.9	6/29/2011	97.08	585.5	1	0.50
5-4	-0.7	30.2	0.1	25.5	6/29/2011	97.40	594.8	2	-4.49
4-27	-0.5	30.4	0.2	25.6	6/29/2011	96.67	600.4	1	1.37
5-17	-0.5	30.4	0.2	25.6	6/29/2011	96.39	601.7	1	2.60
5-5	-0.5	30.4	0.1	25.7	6/29/2011	97.20	605.3	2	4.57
5-18	-0.4	30.5	0.2	25.7	6/29/2011	96.51	615.5	2	-0.33
5-6	-0.8	30.0	0.1	25.3	6/29/2011	98.62	621.2	1	-5.18
5-7	-0.7	30.2	0.1	25.5	6/29/2011	96.42	630.3	2	0.51
5-8	-0.8	30.0	0.1	25.3	6/29/2011	95.86	642.3	1	3.64
5-9	-0.3	30.6	0.1	25.8	6/29/2011	97.02	646.8	2	0.72
5-20	-0.7	30.2	0.2	25.4	6/29/2011	96.39	656.1	1	-3.95
5-10	-0.4	30.5	0.1	25.7	6/29/2011	96.35	658.8	2	-2.92
5-11	-0.4	30.5	0.1	25.8	6/29/2011	96.36	666.9	2	1.95
5-22	-0.5	30.4	0.2	25.6	6/29/2011	97.21	678.3	2	1.83
5-23	-0.9	30.0	0.2	25.2	6/29/2011	97.17	689.1	1	-0.79
5.5-1	-1.3	29.6	0.3	26.4	2/14/2014	97.70	699.5	1	-5.83
5-14	-0.9	30.0	0.1	25.2	6/29/2011	96.52	700.0	1	-5.41
5-24	-0.8	30.1	0.2	25.3	6/29/2011	96.95	703.0	2	-0.73
5.5-2	-0.9	30.0	0.3	26.8	2/14/2014	98.10	710.3	2	3.55
5-16	-0.8	30.0	0.1	25.3	6/29/2011	96.63	720.4	2	1.65
5.5-3	-0.8	30.0	0.3	26.8	2/14/2014	97.70	723.7	1	1.72
5.5-3	-0.8	30.0	0.3	26.8	2/14/2014	97.70	730.5	1	-1.57
5-26	-1.0	29.9	0.2	25.1	6/29/2011	96.45	731.8	1	-1.55

(Continued)



Table 2. (Continued)

Analysis Name	$\delta^{18}\text{O}_{\text{VPDB}}^{**}$ (‰)	$\delta^{18}\text{O}_{\text{VSMOW}}^*$ (‰)	Error <sup>c</sup> (2s.d.)	$\delta^{18}\text{O}_{\text{Raw}}^{\wedge}$ (‰)	Date	RelativeYield <sup>e</sup> (%)	Dist. <sup>k</sup> (µm)	Pit quality	CLFM Greyscale <sup>^</sup>
5–28	-1.1	29.8	0.2	25.0	6/29/2011	97.35	752.5	1	3.17
5.5–5	-0.5	30.4	0.3	27.2	2/14/2014	98.50	753.0	2	2.86
5.5–7	-0.6	30.3	0.3	27.1	2/14/2014	97.40	759.6	2	2.56
5.5–6	-0.2	30.7	0.3	27.5	2/14/2014	97.30	762.8	1	2.86
5.5–8	-0.7	30.2	0.3	27.0	2/14/2014	97.80	773.7	2	-4.64
5–29	-0.6	30.2	0.2	25.4	6/29/2011	96.17	776.7	1	-4.83
5.5–9	-0.5	30.4	0.3	27.2	2/14/2014	97.00	783.8	2	2.91
5.5–10	-0.4	30.5	0.3	27.3	2/14/2014	97.90	792.8	2	3.67
5.5–11	0.1	31.0	0.3	27.8	2/14/2014	95.30	840.6	1	0.46
6–2	0.0	30.9	0.3	27.6	2/14/2014	96.00	848.7	1	1.70
5.5–12	-0.3	30.7	0.3	27.4	2/14/2014	95.40	849.6	1	1.16
6–3	0.0	30.9	0.3	27.6	2/14/2014	95.00	858.3	1	0.44
5.5–13	-0.4	30.5	0.3	27.2	2/14/2014	96.20	866.4	1	3.01
6–4	-0.1	30.8	0.3	27.6	2/14/2014	95.40	875.6	1	1.75
5.5–14	0.0	30.9	0.3	27.6	2/14/2014	96.60	885.1	1	-3.61
6–6	-0.8	30.0	0.4	27.0	2/14/2014	98.20	922.0	2	0.99
6–7	-1.0	29.9	0.4	26.8	2/14/2014	98.40	937.9	1	-1.70
7–1	-0.5	30.4	0.3	27.6	2/14/2014	97.50	938.8	1	-1.34
6–8	-0.3	30.6	0.4	27.5	2/14/2014	98.30	950.9	1	3.56
7–3	0.1	31.0	0.3	28.2	2/14/2014	97.30	953.3	1	2.56
6–9	-0.6	30.3	0.4	27.2	2/14/2014	98.60	964.4	2	-3.09
7–4	-0.7	30.2	0.3	27.5	2/14/2014	97.20	971.9	2	-2.15
7–5	-0.4	30.5	0.3	27.7	2/14/2014	97.20	984.5	1	4.88
6–11	-0.4	30.5	0.4	27.4	2/14/2014	98.90	992.6	1	-2.44
7–6	-0.4	30.5	0.3	27.8	2/14/2014	97.60	994.1	1	-3.60
7–7	-0.5	30.4	0.3	27.6	2/14/2014	97.40	1005.5	1	-1.61

(Continued)

Table 2. (Continued)

Analysis Name	$\delta^{18}\text{O}_{\text{VPDB}}^{**}$ (‰)	$\delta^{18}\text{O}_{\text{VSMOW}}^*$ (‰)	Error <sup>†</sup> (2s.d.)	$\delta^{18}\text{O}_{\text{Raw}}^{\wedge}$ (‰)	Date	RelativeYield <sup>€</sup> (%)	Dist. <sup>κ</sup> (μm)	Pit quality	CLFM Greyscale <sup>^</sup>
6–13	-0.3	30.6	0.4	27.5	2/14/2014	99.50	1020.3	1	3.47
7–9	0.1	31.0	0.3	28.2	2/14/2014	96.70	1021.3	1	3.16
6–14	-0.4	30.5	0.4	27.4	2/14/2014	99.50	1025.1	2	1.32
7–10	-0.5	30.4	0.3	27.6	2/14/2014	97.20	1034.7	1	-1.13
8–1	-0.4	30.5	0.4	27.8	2/14/2014	98.70	1038.0	2	-1.08
7–11	-0.6	30.3	0.2	27.6	2/14/2014	98.20	1041.0	1	-2.69
6–16	-0.5	30.4	0.4	27.3	2/14/2014	99.40	1042.5	2	-2.41
8–2	-0.5	30.4	0.4	27.8	2/14/2014	97.90	1047.6	1	0.42
7–12	0.1	31.0	0.2	28.2	2/14/2014	97.90	1048.8	1	1.35
8–3	-0.5	30.4	0.4	27.8	2/14/2014	98.90	1058.1	1	2.00
8–4	-0.9	30.0	0.4	27.3	2/14/2014	98.40	1067.4	1	-3.70
7–14	-0.3	30.6	0.2	27.9	2/14/2014	98.50	1072.2	1	-2.21
7–15	-0.4	30.5	0.2	27.7	2/14/2014	99.10	1077.1	1	-0.51
7–16	-0.3	30.6	0.2	27.8	2/14/2014	98.60	1085.5	1	1.27
8–6	-1.1	29.8	0.4	27.1	2/14/2014	99.00	1089.1	1	1.47
8–7	-1.4	29.5	0.4	26.8	2/14/2014	99.80	1099.9	1	-2.15
7–18	-0.8	30.1	0.2	27.3	2/14/2014	98.30	1104.7	1	-1.97
8–8	-0.3	30.6	0.4	27.9	2/14/2014	98.90	1112.5	1	-2.00
7–19	-0.7	30.2	0.2	27.5	2/14/2014	98.70	1117.3	1	-0.15
8–9	-0.8	30.1	0.4	27.5	2/14/2014	98.00	1125.1	1	1.94
7–20	-0.3	30.6	0.2	27.9	2/14/2014	98.40	1128.7	2	1.83
9–2	-0.4	30.5	0.1	26.9	2/15/2014	98.80	1153.1	1	-3.63
8–12	-0.2	30.7	0.4	27.3	2/15/2014	98.70	1157.0	1	-2.10
8–13	-0.2	30.7	0.4	27.3	2/15/2014	98.50	1166.3	1	4.64
9–3	0.0	30.9	0.1	27.3	2/15/2014	98.40	1169.6	2	2.89
9–4	0.2	31.1	0.1	27.5	2/15/2014	98.10	1175.6	1	3.03

(Continued)

Table 2. (Continued)

Analysis Name	$\delta^{18}\text{O}_{\text{VPDB}}^{**}$ (‰)	$\delta^{18}\text{O}_{\text{VSMOW}}^*$ (‰)	Error <sup>c</sup> (2s.d.)	$\delta^{18}\text{O}_{\text{Raw}}^{\wedge}$ (‰)	Date	RelativeYield <sup>e</sup> (%)	Dist. <sup>k</sup> (µm)	Pit quality	CLFM Greyscale <sup>^</sup>
8–15	-0.1	30.8	0.4	27.4	2/15/2014	98.30	1176.2	1	2.26
9–5	-0.1	30.8	0.1	27.3	2/15/2014	98.60	1179.2	1	2.67
8–16	-0.6	30.3	0.4	26.9	2/15/2014	98.90	1190.6	1	-3.25
9–6	-0.4	30.5	0.1	27.0	2/15/2014	98.30	1193.6	1	-4.05
9–7	-0.3	30.6	0.1	27.1	2/15/2014	97.80	1199.3	1	-0.53
8–17	-0.5	30.4	0.4	27.0	2/15/2014	99.00	1199.6	2	-0.86
9–8	-0.5	30.4	0.1	26.9	2/15/2014	99.00	1214.1	2	1.21
8–18	0.0	30.9	0.4	27.4	2/15/2014	100.00	1215.0	1	1.77
8–19	0.3	31.2	0.4	27.8	2/15/2014	99.90	1225.8	1	-6.13
9–9	0.6	31.5	0.1	28.0	2/15/2014	99.90	1226.7	1	-6.46
8–20	0.2	31.1	0.4	27.7	2/15/2014	98.70	1229.1	2	-4.94
10–1	0.4	31.3	0.3	27.7	2/15/2014	98.70	1234.2	1	-1.46
9–10	0.9	31.8	0.1	28.3	2/15/2014	99.60	1235.1	1	-1.02
10–2	0.4	31.3	0.3	27.7	2/15/2014	99.10	1241.1	1	3.50
9–11	0.1	31.0	0.3	27.5	2/15/2014	99.00	1242.0	1	2.87
10–3	0.2	31.1	0.3	27.5	2/15/2014	99.20	1247.4	2	2.01
9–13	-0.3	30.6	0.3	27.1	2/15/2014	98.80	1258.2	2	-0.05
10–5	-0.6	30.3	0.3	26.7	2/15/2014	98.30	1268.2	1	1.61
9–14	-0.7	30.2	0.3	26.6	2/15/2014	98.80	1269.7	1	1.23
10–6	-0.7	30.2	0.3	26.6	2/15/2014	98.40	1282.3	1	-0.19
9–16	-1.2	29.7	0.3	26.1	2/15/2014	97.30	1285.9	2	-0.82
10–7	-0.4	30.5	0.3	27.0	2/15/2014	98.00	1288.0	1	-0.04
9–18	-0.8	30.1	0.3	26.5	2/15/2014	99.10	1304.8	1	-1.80
10–9	0.0	30.9	0.3	27.3	2/15/2014	98.00	1309.9	1	-1.43
9–19	-0.7	30.2	0.3	26.6	2/15/2014	98.50	1311.7	1	-3.00
9–20	-0.5	30.4	0.3	26.9	2/15/2014	98.90	1321.3	2	1.02

(Continued)

Table 2. (Continued)

Analysis Name	$\delta^{18}\text{O}_{\text{VPDB}}^{**}$ (‰)	$\delta^{18}\text{O}_{\text{VSMOW}}^*$ (‰)	Error <sup>†</sup> (2s.d.)	$\delta^{18}\text{O}_{\text{Raw}}^{\wedge}$ (‰)	Date	RelativeYield <sup>€</sup> (%)	Dist. <sup>κ</sup> (μm)	Pit quality	CLFM Greyscale <sup>^</sup>
10–11	0.4	31.3	0.3	27.7	2/15/2014	98.70	1331.6	2	-0.85
10–12	0.1	31.0	0.3	27.3	2/15/2014	98.50	1337.3	2	0.32
10–13	-0.1	30.8	0.3	27.2	2/15/2014	98.70	1342.7	1	3.25
10–14	-0.6	30.3	0.3	26.7	2/15/2014	99.10	1352.9	2	-3.02
10–15	0.1	31.0	0.3	27.4	2/15/2014	98.30	1365.2	2	1.26
10–17	0.4	31.3	0.3	27.7	2/15/2014	98.50	1376.3	1	1.45
11–1	0.2	31.1	0.4	27.5	2/15/2014	98.10	1381.1	1	2.03
10–18	-0.2	30.7	0.3	27.0	2/15/2014	98.60	1382.0	1	1.27
12–1	0.5	31.5	0.3	28.0	2/15/2014	98.00	1384.0	1	-0.19
11–2	-0.1	30.8	0.4	27.2	2/15/2014	98.80	1384.1	2	-0.30
10–19	-0.1	30.8	0.3	27.2	2/15/2014	98.90	1388.3	1	-5.04
10–21	0.3	31.2	0.4	27.6	2/15/2014	99.30	1396.9	1	-2.10
10–20	0.1	31.0	0.3	27.4	2/15/2014	98.10	1398.0	2	-2.02
12–2	0.0	30.9	0.3	27.4	2/15/2014	98.10	1398.6	1	-1.42
11–3	-0.3	30.6	0.4	27.1	2/15/2014	98.40	1399.8	1	-0.08
12–3	0.5	31.4	0.3	27.9	2/15/2014	97.90	1409.5	1	3.24
10–22	0.0	30.9	0.4	27.4	2/15/2014	98.60	1411.5	2	3.04
11–4	0.3	31.3	0.4	27.7	2/15/2014	97.90	1413.3	1	2.66
11–6	0.3	31.2	0.4	27.6	2/15/2014	98.00	1421.7	1	-1.09
12–4	0.3	31.2	0.3	27.7	2/15/2014	97.80	1427.0	1	0.64
10–24	-0.4	30.5	0.4	26.9	2/15/2014	100.40	1430.1	1	1.69
12–5	0.4	31.3	0.3	27.8	2/15/2014	97.50	1437.9	1	-1.22
11–7	-1.0	29.9	0.3	26.4	2/15/2014	99.30	1438.8	2	-1.57
11–8	0.2	31.1	0.3	27.6	2/15/2014	99.20	1444.5	1	-4.31
12–6	0.7	31.6	0.3	28.1	2/15/2014	97.90	1450.8	1	-0.77
11–9	0.5	31.4	0.3	27.9	2/15/2014	98.70	1455.9	2	3.31

(Continued)

Table 2. (Continued)

Analysis Name	$\delta^{18}\text{O}_{\text{VPDB}}^{**}$ (‰)	$\delta^{18}\text{O}_{\text{VSMOW}}^*$ (‰)	Error <sup>£</sup> (2s.d.)	$\delta^{18}\text{O}_{\text{Raw}}^{\wedge}$ (‰)	Date	RelativeYield <sup>€</sup> (%)	Dist. <sup>κ</sup> (μm)	Pit quality	CLFM Greyscale <sup>^</sup>
11–10	0.6	31.6	0.3	28.1	2/15/2014	98.60	1458.4	2	3.19
12–7	-0.3	30.6	0.3	27.1	2/15/2014	97.50	1480.7	1	-0.73
11–13	-0.5	30.4	0.3	26.9	2/15/2014	99.30	1481.5	2	-0.41
12–8	-0.4	30.5	0.3	27.0	2/15/2014	98.40	1482.1	1	-0.24
11–14	0.0	30.9	0.3	27.4	2/15/2014	98.80	1497.1	1	1.41
11–15	0.2	31.1	0.3	27.6	2/15/2014	98.20	1504.0	2	1.13
11–16	-0.2	30.7	0.3	27.2	2/15/2014	98.8	1506.7	2	1.23
11–18	-0.3	30.6	0.3	27.1	2/15/2014	98.7	1523.3	2	0.77

Analysis names refer to Transect#-Pit#.

\*\* Conversion from VSMOW and corrected to aragonite (-0.98)  $\delta^{18}\text{O}_{\text{VPDB}} = (\delta^{18}\text{O}_{\text{VSMOW}} - 30.91)/1.03091$ .

\* Value adjusted by bracketing standard and corrected to aragonite.

<sup>^</sup> Value reported vs. VSMOW  $\delta^{18}\text{O}_{\text{raw}} = \{({}^{18}\text{O}/{}^{16}\text{O} \text{ measured}/0.00200520) - 1\} * 1000$

<sup>£</sup> Precision for  $\delta^{18}\text{O}_{\text{VPDB}}$  measurements derived from 2 times standard deviation of eight bracketing standards.

<sup>€</sup> Yield relative to the mean yield of 8 bracketing standards.

<sup>κ</sup> Distance values in micrometers perpendicular to visible banding to center of analysis pit.

<sup>^</sup> Normalized CLFM grey scale value from averaged line of pixels parallel to growth banding in CLFM image for pit location with lowess regression removed to correct for trends in brightness across and between images. Low values are dark portions of growth bands and high values are bright portion.

doi:10.1371/journal.pone.0153890.t002

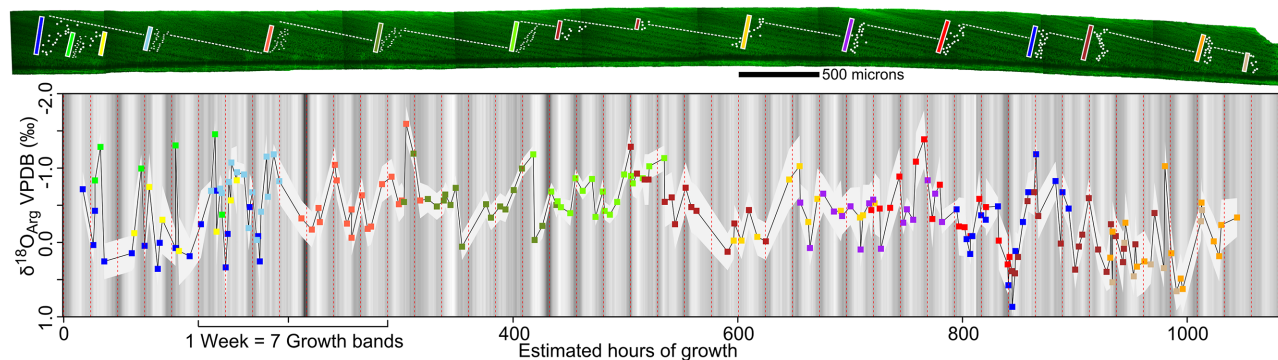


**Fig 5. SIMS results and CLFM brightness for transects perpendicular to banding in the outer prismatic layer of the wild-caught *Nautilus macromphalus* (AMNH 105621).** SIMS analysis and CLFM imaging was done on this 8 mm long portion of vacuum roasted and polished *Nautilus macromphalus* shell. The background grayscale is based on the residual CLFM brightness after lowess regression to correct for differences in brightness within and between images. Oxygen isotope ratios are plotted against hours of growth, assuming that each dark-light-dark cycle is 24 hours. The most recently precipitated shell is at time 0. Overlapping transects are color coded to show where correlation across the shell was carried out to produce the composite record. Transect locations are highlighted on the CLFM image of the outer prismatic layer. Correlation shows agreement within instrumental precision between transects correlated across the shell. There is considerable oxygen isotope variability within daily individual growth bands and across multiple bands. A higher resolution map of the shell surface is available in the supplementary information (S1 Fig).

doi:10.1371/journal.pone.0153890.g005

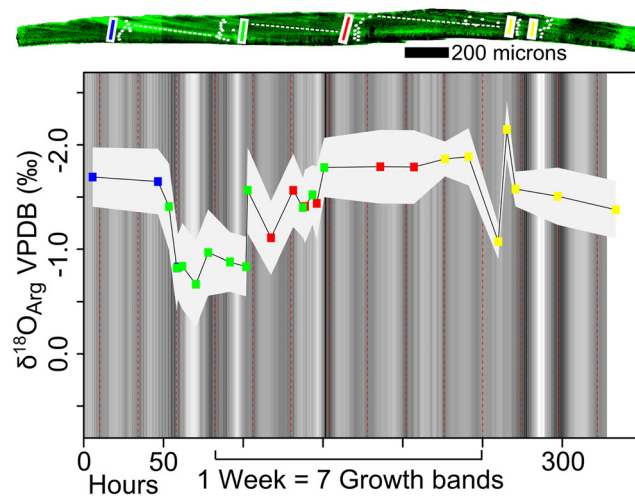


**Fig 6. SIMS results and CLFM brightness for transects perpendicular to banding in the outer prismatic layer of the aquarium-reared *Nautilus belauensis* (AMNH 102555).** SIMS analysis and CLFM imaging was done on this 3-mm long portion of vacuum roasted and polished *Nautilus belauensis* shell. The background grayscale is based on the residual CLFM brightness after lowess regression to correct for differences in brightness across and between images. Oxygen isotope ratios are plotted against hours of growth, assuming that each dark-light-dark cycle is 24 hours and the scales of the x and y axes match those of Fig 5. The most recently precipitated shell is at time 0. Overlapping transects are color coded to show where correlation across the shell was done to produce the composite record. Transect locations are highlighted on the CLFM image of the outer prismatic layer. Correlation shows general agreement within instrumental precision between transects correlated across the shell. Finding variability in this sample is particularly interesting because it is one of three individuals that is often cited as an example of *Nautilus* precipitating oxygen in isotopic equilibrium with seawater [12]. The positive shift in  $\delta^{18}\text{O}_{\text{Arg}}$  that takes place over several days is attributed to evaporation of ~8 liters of water from the 80 L incubation tank in which this individual was living [45,47,76]. A higher resolution map of the shell surface is available in the supplementary information (S2 Fig).

doi:10.1371/journal.pone.0153890.g006

## Discussion

### Growth banding

Growth bands that are observed in CLFM, UV, and plain light images (Figs 1 and 3) in both *Nautilus* are interpreted to occur daily. Each band is delimited by a repeated pattern in the amount of organic matter relative to aragonite in the shell, which is most clearly imaged in CLFM as repeated patterns in the luminescence of the shell (Figs 1, 3, 4, 5 and 6). Similar growth banding on a daily timescale has been observed in gastropods reared in aquaria [28]. The apertural growth rates calculated from growth band width range from 104 to 308  $\mu\text{m}/\text{day}$  in the wild-caught *Nautilus macromphalus* and from 65 to 160  $\mu\text{m}/\text{day}$  in the aquarium-reared *Nautilus belauensis*. The width of growth banding within the prismatic layer visible by CLFM in *Nautilus* has not been previously reported in the literature; however, apertural growth rate has been [3,20,21,42,72–74,77,78]. Growth rates for *Nautilus* grown in aquaria range from 0 to 600  $\mu\text{m}/\text{day}$  [42] with an average of 158  $\mu\text{m}/\text{day}$  across nine studies, although abnormal shell growth in aquaria is common [21]. The similarity between growth rates determined from band width and published values suggest that the intraprismatic banding is daily in *Nautilus*. The trend across 7–8 growth bands toward higher  $\delta^{18}\text{O}$  values in the aquarium-reared sample (Fig 6) also suggests daily growth bands, because the duration of the pattern may from evaporative enrichment in the aquarium over one week as reported in the aquarium management procedure [45,47]. Shell growth across a wide range of depths can be inferred from the 2.5‰  $\delta^{18}\text{O}$  range across the wild-caught sample, which is larger than ranges reported for sampling across

entire shells [1,4,8,11]. Variation within growth bands of up to 1.5‰ indicate a range of temperatures of at least ~5°C, which can likely only be captured if growth is continuous in a mobile organism at the SIMS sampling resolution (~7 hours for 10 μm growth). If growth was not continuous across all depths or growth rate varied widely with temperature,  $\delta^{18}\text{O}$  should not vary within or across the sampled growth bands by as much as we have detected. However, because our analyses do include some amount of time-averaging, truncation or slowing of growth during extremely shallow or deep excursions cannot be excluded as a possibility. Because growth banding can be interpreted to be daily and growth rate variation within individual days cannot be reliably inferred, both Figs 5 and 6 have been scaled so that each dark—light—dark band is equal to 24 hours and growth rate is uniform within individual days.

### $\delta^{18}\text{O}_{\text{Arg}}$ variability in *Nautilus macromphalus* and *Nautilus belauensis*

SIMS analysis of both the wild-caught sample and the aquarium-reared sample found  $\delta^{18}\text{O}_{\text{Arg}}$  variation within the outer prismatic layer of aragonite, but the character of variability is strikingly different between the two samples (Figs 5 and 6). The aquarium-reared *Nautilus belauensis* (AMNH 102555) has a prominent gradual increase in the  $\delta^{18}\text{O}_{\text{Arg}}$  values across ~7 growth bands and then an abrupt decrease over ~1 growth band (at 75 hours, Fig 6). This gradual increase can be explained by evaporative increase of  $\delta^{18}\text{O}$  [76] followed by a sudden decrease during recharge and replacement with lower  $\delta^{18}\text{O}$  water. This refill and replacement cycle occurred once weekly over approximately 8 hours to prevent shocking the *Nautilus*, with water coming from a salt-water well [45,47]. Experimental evaporation studies where the  $\delta^{18}\text{O}$  of residual liquid was measured after evaporation under controlled-humidity air (at 0, 20, 51% humidity, 19.6 to 20°C) suggest that ~10% evaporation from the tank will produce a shift of about +1‰ in the  $\delta^{18}\text{O}$  of aquarium water [76] on the timescale of 7 days. Subsequent refilling will cause a drop of comparable magnitude in ~8 hours because water is coming from a groundwater source that likely has a uniform  $\delta^{18}\text{O}$ . This evaporation and refilling is the main influence on the  $\delta^{18}\text{O}_{\text{Arg}}$  of the aquarium-reared sample, because temperature was kept constant at 22°C ±1°C (~0.4‰) [12,45,47]. Variation in the  $\delta^{18}\text{O}_{\text{Arg}}$  of the wild-caught *Nautilus macromphalus* (AMNH 105621) is greater within individual bands and of greater magnitude across fewer bands than the aquarium-reared individual (Figs 5 vs 6), which suggests a different mechanism for the formation of the variability.

### Oxygen isotope patterns and depth migration

It is widely accepted that changing habitat depth through weeks to years of an individual cephalopod's lifetime can be interpreted from patterns in  $\delta^{18}\text{O}_{\text{Arg}}$  caused by the thermal gradient in the water column [1,2,5–9,11,12,79–82]. Variability in our new *in situ* measurements of  $\delta^{18}\text{O}_{\text{Arg}}$  can be interpreted as sub-daily depth-migration behavior if the following three criteria are met: 1)  $\delta^{18}\text{O}_{\text{Arg}}$  variation is largely decoupled from physiological variation (e.g. concentration of organic matter controlling CLFM fluorescence) 2) both high and low  $\delta^{18}\text{O}_{\text{Arg}}$  values are observed within individual bands (suggesting different depths within one day), and 3) the range of  $\delta^{18}\text{O}_{\text{Arg}}$  variation falls near or within expected values from depth constraints and water column conditions near New Caledonia (~20°C or ~4.0‰ between 0 to 750 m, Fig 2 [1,15]). These three criteria provide a consistent test for the presence or absence of the depth migration behavior in modern and fossil cephalopods. Testing all three criteria requires collecting a dataset that combines high precision *in situ* isotope analyses with a physical record of growth, but does not require shell to be precipitated in equilibrium, only a uniform vital effect that does not vary within days.

If  $\delta^{18}\text{O}_{\text{Arg}}$  covaries strongly with physiological variation, such as growth banding, then variation in  $\delta^{18}\text{O}_{\text{Arg}}$  could be explained as a vital effect that fractionates carbonate during precipitation, where varying rates of precipitation would be related to the ratio of organic matter to carbonate in the shell and therefore CLFM brightness [83]. However, in the wild-caught and aquarium reared *Nautilus*,  $\delta^{18}\text{O}_{\text{arg}}$  varies within individual growth bands but does not covary with CLFM brightness (Figs 5 and 6), which suggests independent causes for growth banding and  $\delta^{18}\text{O}_{\text{Arg}}$  variability. Daily growth banding is caused by a physiological rhythm that is paced by a circadian clock [29,30,43]. A physiological pattern is expected to be regular because it is not controlled by the presence or absence of food or predators, but is controlled by the physical mechanisms of shell formation, in this case the production of the organic matter that is incorporated into the shell during precipitation. A behavioral pattern is not expected to perfectly covary with the circadian clock because it is the product of response of the individual *Nautilus* based on stochastic external stimuli, such as the appearance of food or predators [84]. This response to external stimuli is apparent in existing telemetry data because individuals are not at the same depth at the same time on different days [17–19]. Aquaria studies of other cephalopods (*Octopus*) demonstrate idiosyncratic timing of the activity of individuals even in a nocturnal population [85]. In the wild-caught *Nautilus macromphalus* (AMNH 105621), growth banding visible in CLFM is a recorder of a physiological rhythm and measured  $\delta^{18}\text{O}_{\text{Arg}}$  is a recorder of migration through a water column with a large ( $\sim 20^\circ\text{C}$ ) thermal gradient across possible living depths (0–750 m) (Fig 2). In the aquarium-reared *Nautilus belauensis* (AMNH 102555), growth banding records a physiological rhythm, and the  $\delta^{18}\text{O}_{\text{arg}}$  records changing aquarium conditions.

Oxygen isotope variation larger than instrumental precision (95% CI) within or across individual bands is observed in 27 of the 41 bands with two or more analyses in them (Fig 6). Variation beyond precision strongly suggests that this *Nautilus macromphalus* was not staying within constant temperature or  $\delta^{18}\text{O}$  water during shell precipitation. Continuous precipitation within the limits of sampling resolution (10- $\mu\text{m}$  spot  $\sim 7.5$  hours) is suggested by intermediate oxygen isotope values between low and adjacent high values (Fig 6). Cycles that are apparent across several bands may be due to time averaging from the SIMS pits, aliasing of the  $\delta^{18}\text{O}$  record due to pit spacing, and pit-time averaging, or they could be a real record of a pattern of depth migration. It is also possible that the complete range of  $\delta^{18}\text{O}_{\text{arg}}$  was not sampled due to slowed growth at either cold or hot temperatures [86].

To create a  $\delta^{18}\text{O}_{\text{arg}}$  range of 2.5‰ (0.9 to -1.6‰ VPDB) in the wild-caught sample, the *Nautilus macromphalus* must have crossed a temperature gradient of  $\sim 12^\circ\text{C}$  based on Eq 1, assuming constant  $\delta^{18}\text{O}_{\text{SW}}$ . When temperatures are calculated using a  $\delta^{18}\text{O}_{\text{SW}}$  value of 0.5‰, they range from 27.6 to 15.5°C. The warm temperature is high for reported seawater temperature values (high of 26.3 Fig 2, [15]), but it is still possible for the *Nautilus* to have experienced this temperature without immediately dying [42,87,88] and *Nautilus macromphalus* have been observed in shallow water (<10 m) near New Caledonia [87]. This temperature range suggests the individual crossed at least  $\sim 400$  m depth assuming a change of  $0.3^\circ\text{C}/\text{m}$ . This range of depth change over the 45 days is similar to that observed in shorter observation intervals by remote telemetry [17–19] and photocapture traps [20]. The range in  $\delta^{18}\text{O}$  is larger than that observed in adult shells by conventional analysis techniques [1–6].

## Comparison to remote telemetry migration data

The pattern of oxygen isotope variability within bands can be compared to patterns of depth migration recorded by remote telemetry. Fig 7A illustrates the  $\delta^{18}\text{O}$  pattern calculated for one of the four individuals tracked by Ward *et al.* [17]. Dunstan *et al.* [19] reported more chaotic



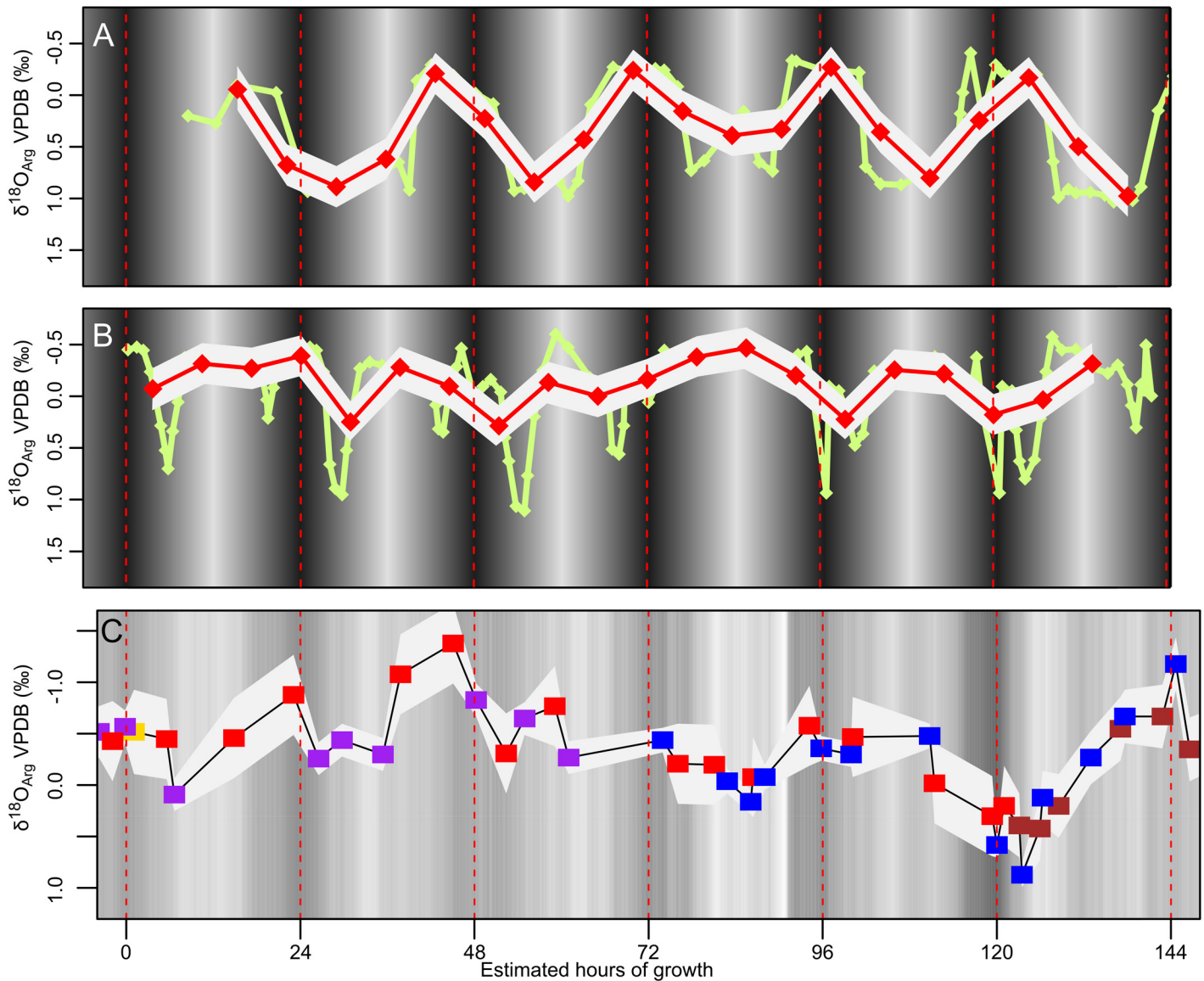


**Fig 7. A comparison of SIMS measured  $\delta^{18}\text{O}_{\text{Arg}}$  to telemetry results that have been converted to  $\delta^{18}\text{O}_{\text{Arg}}$ .** Telemetry is done using ultrasonic transmitters that are attached to the dorsal shell of *Nautilus* and are monitored from boats or stationary underwater receivers [17–19]. SIMS results can be compared to telemetry records if water temperatures and  $\delta^{18}\text{O}$  are known, growth is continuous, and time averaging is calculated. Green lines in A and B are telemetry data converted to  $\delta^{18}\text{O}_{\text{Arg}}$  assuming a thermal gradient of  $0.3^\circ\text{C}/\text{m}$ , with a constant  $\delta^{18}\text{O}_{\text{sw}}$  of  $0.5\text{‰}$  (VSMOW) and using Eq 1. Overlying red lines are hypothetical SIMS data approximate time averaging from a  $10\text{-}\mu\text{m}$  spot diameter SIMS spot assuming  $35\ \mu\text{m}/\text{day}$  growth. The gray background is the 2SD instrumental precision envelope around the SIMS analyses. A) Regular shallow-deep migrations observed in *Nautilus belauensis* off Palau [17] would likely leave a SIMS result with regular variability. B) Rapid excursions to depths at dawn and dusk, like those observed in *N. pompilius* off Osprey Reef, Australia [19] would leave less variability in the SIMS results due to the effects of time averaging. C) Actual SIMS results for the wild-caught *Nautilus macromphalus* from New Caledonia suggest that depth migration can be detected; however, there is not a regular migratory pattern like that observed at Palau. A different style of depth migration pattern, influenced by the local bathymetry or cover availability, could explain the differences between the telemetry data and the SIMS measurements. The  $\delta^{18}\text{O}_{\text{arg}}$  variation measured by SIMS in this study shows that the wild-caught sample spent significant amounts of time in both shallow and deep water, a behavior more similar to that observed by Ward *et al.* [17] and Carlson *et al.* [18] near Palau (fringing reef) than that observed by Dunstan *et al.* [19] near Osprey Reef (submerged atoll), Australia. Dunstan *et al.* [19] suggest that the behavioral difference between Osprey Reef and Palau is due to available hiding locations, and therefore it is possible that hiding locations on the fore-reef of the fringing reef near New Caledonia are less abundant than those on Osprey Reef. Differences in behavior could also be due to other factors of location or differences between species.

doi:10.1371/journal.pone.0153890.g007

depth migratory patterns (Fig 7B). Time averaging from SIMS sampling would truncate a depth migration record and reduce the apparent amplitude of migration and duration at depth (Fig 7A and 7B) in the same way that time averaging of stable isotope sampling can truncate seasonal temperature variability in bivalves [86]. For instance, if an individual was stationary at a depth where  $\delta^{18}\text{O}_{\text{Arg}}$  was 1.0‰ (VPDB) and then there was a short (<3 hour) migration to a depth where  $\delta^{18}\text{O}_{\text{Arg}}$  was 2.0‰ (VPDB), the difference between a point in the stationary depth and the migration depth would be ~0.4‰ assuming 7 hours/pit time averaging. Thus, a more chaotic migration pattern with very short excursions to extreme depths when measured by SIMS would have a greater dampening of  $\delta^{18}\text{O}_{\text{arg}}$  excursions because the domains showing highest or lowest  $\delta^{18}\text{O}_{\text{arg}}$  cannot be fully resolved by the 10  $\mu\text{m}$  SIMS analysis pit (Fig 7B).

### Implications of sub-daily isotope sampling in Cephalopods

The capability to precisely measure sub-daily variation of  $\delta^{18}\text{O}$  within rapidly accreted biominerals presents new avenues for biological, paleobiological, and paleoecological research. Isotope analyses of well-preserved fossil cephalopods (i.e. nacreous microstructure preserved [89]) have been used to interpret ontogenetic habitat change and mean living depth [7–9,11,44,79,80,89–91]. This study suggests that estimating the activity and mobility of extinct cephalopods is possible by analyzing  $\delta^{18}\text{O}$  within growth bands in samples that preserve nacreous microstructure and the original mineralogy. These techniques can be used to test morphological hypotheses about the swimming ecology of ammonites [81,92,93]. Inferring depth migration behavior from  $\delta^{18}\text{O}$  in fossil material is a new approach for studies of marine ecology for situations where: 1) growth banding can be imaged to provide a physiological chronometer, and 2) a sufficient temperature or salinity gradient within ambient waters is present, which when analyzing fossil material can be determined by data from foraminifera or other benthic and planktonic organisms [91].

### Conclusions

SIMS analyses within visible growth banding of mollusk shells attain high spatial and analytical precision allowing us to measure a greater range in  $\delta^{18}\text{O}$  than that measured in adult shells using conventional analyses that average days to weeks of growth. Our new data record a depth-migratory signal in the  $\delta^{18}\text{O}$  values of the wild-caught *Nautilus macromphalus* shell. The width of growth banding visible by confocal laser fluorescence microscopy suggests that the bands are daily and the 10- $\mu\text{m}$  diameter of SIMS pits used in this study yield an average time resolution of ~8 hours. Analysis of the aquarium-reared *Nautilus belauensis* shell suggests equilibrium precipitation, but also indicates that more controlled aquarium rearing studies are necessary. Combined, the results of this study serve as an example for the investigation of depth migration in fossil cephalopods. These results from *Nautilus* strongly suggest that high-resolution sampling across growth banding with SIMS can elucidate a signal of depth migration behavior by externally shelled cephalopods.

### Supporting Information

**S1 Fig.** SEM and CLFM images of transects on *Nautilus macromphalus*, AMNH 105621. (PDF)

**S2 Fig.** SEM and CLFM images of transects on *Nautilus belauensis*, AMNH 102555. (PDF)

**S1 Table.** Table of all SIMS analyses including rejected values for sample *Nautilus macromphalus*, AMNH 105621. Complete data table of analyses in the outer prismatic layer of the

wild-caught *Nautilus macromphalus* including bracketing standards and aragonite standard. (XLSX)

**S2 Table. Table of all SIMS analyses including rejected values for sample *Nautilus belauensis*, AMNH 102555.** Complete data table of analyses in the outer prismatic layer of the aquarium-reared *Nautilus belauensis* including bracketing standards and aragonite standard. (XLSX)

## Acknowledgments

We thank Neil Landman and Royal Mapes for providing samples, discussion, encouragement and inspiration for this project. Mike Spicuzza, Jim Kern, and Brian Hess assisted in sample preparation. Phil Gopon, John Fournelle, Ian Orland, Jason Huberty, and Lance Rodenkirch assisted in imaging the samples. Georgia Wolfe, David Lovelace, Shawn Wallace, Bruce Carlson, and M.M. Yacobucci are thanked for discussion of this project. D. Clay Kelly provided comments on an early copy of this manuscript. We would also like to thank the two anonymous reviewers and Steffen Kiel for their comments that helped improve the manuscript.

## Author Contributions

Conceived and designed the experiments: B JL RK SEP JWV. Performed the experiments: B JL RK. Analyzed the data: B JL RK SEP JWV. Contributed reagents/materials/analysis tools: B JL RK SEP JWV. Wrote the paper: B JL RK SEP JWV.

## References

1. Auclair A-C, Lecuyer C, Bucher H, Sheppard SM. Carbon and oxygen isotope composition of *Nautilus macromphalus*: a record of thermocline waters off New Caledonia. *Chem Geol*. 2004; 207: 91–100. doi: [10.1016/j.chemgeo.2004.02.006](https://doi.org/10.1016/j.chemgeo.2004.02.006)
2. Oba T, Kai M, Tanabe K. Early life history and habitat of *Nautilus pompilius* inferred from oxygen isotope examinations. *Mar Biol*. 1992; 113: 211–217.
3. Cochran JK, Rye DM, Landman NH. Growth rate and habitat of *Nautilus pompilius* inferred from radioactive and stable isotope studies. *Paleobiology*. 1981; 7: 469–480.
4. Ohno A, Miyaji T, Wani R. Inconsistent oxygen isotopic values between contemporary secreted septa and outer shell walls in modern *Nautilus*. *Lethaia*. 2014; doi: [10.1111/let.12109](https://doi.org/10.1111/let.12109)
5. Eichler R, Ristedt H. Isotopic evidence on the early life history of *Nautilus pompilius* (Linné). *Science*. 1966; 153: 734–736. doi: [10.1126/science.153.3737.734](https://doi.org/10.1126/science.153.3737.734) PMID: [17791127](https://pubmed.ncbi.nlm.nih.gov/17791127/)
6. Taylor BE, Ward PD. Stable isotopic studies of *Nautilus macromphalus* Sowerby (New Caledonia) and *Nautilus pompilius* L. (Fiji). *Palaeogeogr Palaeoclimatol Palaeoecol*. 1983; 41: 1–16. doi: [10.1016/0031-0182\(83\)90072-X](https://doi.org/10.1016/0031-0182(83)90072-X)
7. Kruta I, Landman NH, Cochran JK. A new approach for the determination of ammonite and nautilid habitats. *PLoS ONE*. 2014; 9: e87479. doi: [10.1371/journal.pone.0087479](https://doi.org/10.1371/journal.pone.0087479) PMID: [24475295](https://pubmed.ncbi.nlm.nih.gov/24475295/)
8. Landman NH, Rye DM, Shelton KL. Early ontogeny of *Eutrephoceras* compared to recent *Nautilus* and mesozoic ammonites: Evidence from shell morphology and light stable isotopes. *Paleobiology*. 1983; 9: 269–279.
9. Lukeneder A, Harzhauser M, Müllegger S, Piller WE. Ontogeny and habitat change in Mesozoic cephalopods revealed by stable isotopes ( $\delta^{18}\text{O}$ ,  $\delta^{13}\text{C}$ ). *Earth Planet Sci Lett*. 2010; 296: 103–114. doi: [10.1016/j.epsl.2010.04.053](https://doi.org/10.1016/j.epsl.2010.04.053)
10. Schlögl J, Chirat R, Balter V, Joachimski M, Hudáčková N, Quillévéré F. *Aturia* from the Miocene Paratethys: An exceptional window on nautilid habitat and lifestyle. *Palaeogeogr Palaeoclimatol Palaeoecol*. 2011; 308: 330–338. doi: [10.1016/j.palaeo.2011.05.037](https://doi.org/10.1016/j.palaeo.2011.05.037)
11. Zakharov Y, Shigeta Y, Smyshlyayeva O, Popov A, Ignatiev A. Relationship between  $\delta^{13}\text{C}$  and  $\delta^{18}\text{O}$  values of the Recent *Nautilus* and brachiopod shells in the wild and the problem of reconstruction of fossil cephalopod habitat. *Geosci J*. 2006; 10: 331–345. doi: [10.1007/BF02910374](https://doi.org/10.1007/BF02910374)
12. Landman NH, Cochran JK, Rye DM, Tanabe K, Arnold JM. Early life history of *Nautilus*: Evidence from isotopic analyses of aquarium-reared specimens. *Paleobiology*. 1994; 20: 40–51.

13. Tourtelot HA, Rye RO. Distribution of oxygen and carbon isotopes in fossils of Late Cretaceous age, Western Interior region of North America. *Geol Soc Am Bull.* 1969; 80: 1903–1922.
14. House MR. Geographic distribution of *Nautilus* shells. In: Saunders WB, Landman NH, editors. *Nautilus: The Biology and Paleobiology of a Living Fossil.* New York: Plenum Press; 1987. pp. 53–64.
15. Locarnini RA, Mishonov AV, Antonov JI, Boyer TP, Garcia HE, Baranova OK, et al. *World Ocean Atlas 2013, Volume 1: Temperature.* Levitus S, Mishonov A, editors. 2013.
16. Willey A. Contribution to the natural history of the pearly nautilus. (Internet). Cambridge, Eng.: University Press; 1902. Available: <http://www.biodiversitylibrary.org/bibliography/46216>.
17. Ward PD, Carlson B, Weekly M, Brumbaugh B. Remote telemetry of daily vertical and horizontal movement of *Nautilus* in Palau. *Nature.* 1984; 309: 248–250.
18. Carlson B, McKibben JN, deGruy MV. Telemetric Investigation of vertical migration of *Nautilus belauensis* in Palau. *Pac Sci.* 1984; 38: 183–188.
19. Dunstan AJ, Ward PD, Marshall NJ. Vertical distribution and migration patterns of *Nautilus pompilius*. *PLoS ONE.* 2011; 6: e16311. doi: [10.1371/journal.pone.0016311](https://doi.org/10.1371/journal.pone.0016311) PMID: [21364981](https://pubmed.ncbi.nlm.nih.gov/21364981/)
20. Saunders WB. The role and status of *Nautilus* in its natural habitat: Evidence from deep-water remote camera photosequences. *Paleobiology.* 1984; 10: 469–486.
21. Westermann B, Beck-Schildwächter I, Beuerlein K, Kaleta EF, Schipp R. Shell growth and chamber formation of aquarium-reared *Nautilus pompilius* (Mollusca, Cephalopoda) by X-ray analysis. *J Exp Zool A Comp Exp Biol.* 2004; 301A: 930–937.
22. Clark GRI. Organic matrix taphonomy in some molluscan shell microstructures. *Palaeogeogr Palaeoclimatol Palaeoecol.* 1999; 149: 305–312.
23. Mutvei H. On the shells of *Nautilus* and *Spirula*: With notes on shell secretion in non-cephalopod molluscs. *Ark För Zool.* 1964; 16: 221–278.
24. Grégoire C. Ultrastructure of the *Nautilus* Shell. *Nautilus: The Biology and Paleobiology of a Living Fossil.* 1st ed. New York: Plenum Press; 1987. pp. 463–486.
25. Barbin V. Fluctuation in shell composition in *Nautilus* (Cephalopoda, Mollusca): Evidence from cathodoluminescence. *Lethaia.* 1992; 25: 391–400. doi: [10.1111/j.1502-3931.1992.tb01642.x](https://doi.org/10.1111/j.1502-3931.1992.tb01642.x)
26. Loudon ASI. Circadian biology: A 2.5 billion year old clock. *Curr Biol.* 2012; 22: R570–R571. doi: [10.1016/j.cub.2012.06.023](https://doi.org/10.1016/j.cub.2012.06.023) PMID: [22835791](https://pubmed.ncbi.nlm.nih.gov/22835791/)
27. Wijnen H, Young MW. Interplay of circadian clocks and metabolic rhythms. *Annu Rev Genet.* 2006; 40: 409–448. doi: [10.1146/annurev.genet.40.110405.090603](https://doi.org/10.1146/annurev.genet.40.110405.090603) PMID: [17094740](https://pubmed.ncbi.nlm.nih.gov/17094740/)
28. Guzman N, Ball AD, Cuif J-P, Dauphin Y, Denis A, Ortlieb L. Subdaily growth patterns and organo-mineral nanostructure of the growth layers in the calcitic prisms of the shell of *Concholepas concholepas* Bruguière, 1789 (Gastropoda, Muricidae). *Microsc Microanal.* 2007; 13. doi: [10.1017/S1431927607070705](https://doi.org/10.1017/S1431927607070705)
29. Goodwin DH, Flessa KW, Schöne BR, Dettman DL. Cross-calibration of daily growth increments, stable isotope variation, and temperature in the Gulf of California bivalve mollusk *Chione cortezi*: Implications for paleoenvironmental analysis. *PALAIOS.* 2001; 16: 387–398.
30. Schöne BR, Houk SD, Castro ADF, Fiebig J, Oschmann W, Kröncke I, et al. Daily growth rates in shells of *Arctica islandica*: Assessing sub-seasonal environmental controls on a long-lived bivalve mollusk. *PALAIOS.* 2005; 20: 78–92. doi: [10.2110/palo.2003.p03-101](https://doi.org/10.2110/palo.2003.p03-101)
31. de Aguiar DC, Rossi-Wongtschow CLDB, Perez JAA. Validation of daily growth increments of statoliths of Brazilian squid *Doryteuthis plei* and *D. sanpaulensis* (Cephalopoda: Loliginidae). *Bioikos.* 2012; 26. Available: <http://periodicos.puc-campinas.edu.br/seer/index.php/bioikos/article/view/761>.
32. Jackson GD, Moltschanivskij NA. The influence of ration level on growth and statolith increment width of the tropical squid *Sepioteuthis lessoniana* (Cephalopoda: Loliginidae): An experimental approach. *Mar Biol.* 2001; 138: 819–825. doi: [10.1007/s002270000496](https://doi.org/10.1007/s002270000496)
33. Berry WB, Barker RM. Fossil bivalve shells indicate longer month and year in Cretaceous than present. *Nature.* 1968; 217: 938–939.
34. Jones DS. Annual cycle of shell growth increment formation in two continental shelf bivalves and its paleoecologic significance. *Paleobiology.* 1980; 6: 331–340.
35. Jones DS. Sclerochronology: Reading the record of the molluscan shell. *Am Sci.* 1983; 71: 384–391.
36. Jones DS, Arthur MA, Allard DJ. Sclerochronological records of temperature and growth from shells of *Mercenaria mercenaria* from Narragansett Bay, Rhode Island. *Mar Biol.* 1989; 102: 225–234. doi: [10.1007/BF00428284](https://doi.org/10.1007/BF00428284)
37. Thompson I, Jones DS, Dreibelbis D. Annual internal growth banding and life history of the ocean quahog *Arctica islandica* (Mollusca: Bivalvia). *Mar Biol.* 1980; 57: 25–34. doi: [10.1007/BF00420964](https://doi.org/10.1007/BF00420964)

38. Miyaji T, Tanabe K, Matsushima Y, Sato S, Yokoyama Y, Matsuzaki H. Response of daily and annual shell growth patterns of the intertidal bivalve *Phacosoma japonicum* to Holocene coastal climate change in Japan. *Palaeogeogr Palaeoclimatol Palaeoecol*. 2010; 286: 107–120. doi: [10.1016/j.palaeo.2009.11.032](https://doi.org/10.1016/j.palaeo.2009.11.032)
39. Landman NH. Ammonoid growth rhythms. *Lethaia*. 1983; 16: 248–248. doi: [10.1111/j.1502-3931.1983.tb02004.x](https://doi.org/10.1111/j.1502-3931.1983.tb02004.x)
40. Kahn PGK, Pompea SM. Nautiloid growth rhythms and dynamical evolution of the Earth-Moon system. *Nature*. 1978; 275: 606–611. doi: [10.1038/275606a0](https://doi.org/10.1038/275606a0)
41. Doguzhaeva L. Rhythms of ammonoid shell secretion. *Lethaia*. 1982; 15: 385–394. doi: [10.1111/j.1502-3931.1982.tb01703.x](https://doi.org/10.1111/j.1502-3931.1982.tb01703.x)
42. Martin AW, Catala-Stucki I, Ward PD. The growth rate and reproductive behavior of *Nautilus macrophalus*. *Neues Jahrb Geol Palaontologie*. 1978; 156: 207–225.
43. Clark GRI. Growth Lines in invertebrate skeletons. *Annu Rev Earth Planet Sci*. 1974; 2: 77–99.
44. Dennis KJ, Cochran JK, Landman NH, Schrag DP. The climate of the Late Cretaceous: New insights from the application of the carbonate clumped isotope thermometer to Western Interior Seaway macrofossil. *Earth Planet Sci Lett*. 2013; 362: 51–65. doi: [10.1016/j.epsl.2012.11.036](https://doi.org/10.1016/j.epsl.2012.11.036)
45. Carlson B. *Nautilus* hatches at Waikiki Aquarium. *Chambered Naut Newsl*. 1991;
46. Watanabe T, Gagan MK, Corrège T, Scott-Gagan H, Cowley J, Hantoro WS. Oxygen isotope systematics in *Diploastrea heliophora*: new coral archive of tropical paleoclimate. *Geochim Cosmochim Acta*. 2003; 67: 1349–1358. doi: [10.1016/S0016-7037\(02\)01221-8](https://doi.org/10.1016/S0016-7037(02)01221-8)
47. Carlson B, Awai M, Arnold J. Waikiki Aquarium's chambered *Nautilus* reach their first "hatch-day" anniversary. *Hawaii Shell News*. 1992; XL.
48. Crocker KC, DeNiro MJ, Ward PD. Stable isotopic investigations of early development in extant and fossil chambered cephalopods I. Oxygen isotopic composition of eggwater and carbon isotopic composition of siphuncle organic matter in *Nautilus*. *Geochim Cosmochim Acta*. 1985; 49: 2527–2532. doi: [10.1016/0016-7037\(85\)90120-6](https://doi.org/10.1016/0016-7037(85)90120-6)
49. Crick RE, Burkart B, Chamberlain JA, Mann KO. Chemistry of the calcified portions of *Nautilus pompilius*. *J Mar Biol Assoc UK*. 1985; 65: 415–420.
50. Kim S-T, O'Neil JR, Hillaire-Marcel C, Mucci A. Oxygen isotope fractionation between synthetic aragonite and water: Influence of temperature and Mg<sup>2+</sup> concentration. *Geochim Cosmochim Acta*. 2007; 71: 4704–4715. doi: [10.1016/j.gca.2007.04.019](https://doi.org/10.1016/j.gca.2007.04.019)
51. Grossman EL, Ku T-L. Oxygen and carbon isotope fractionation in biogenic aragonite: Temperature effects. *Chem Geol Isot Geosci Sect*. 1986; 59: 59–74. doi: [10.1016/0168-9622\(86\)90057-6](https://doi.org/10.1016/0168-9622(86)90057-6)
52. Coplen TB. Normalization of oxygen and hydrogen isotope data. *Chem Geol Isot Geosci Sect*. 1988; 72: 293–297.
53. Okamoto T. Theoretical modeling of ammonoid morphology. In: Landman N, Tanabe K, Davis R, editors. *Ammonoid Paleobiology*. New York: Plenum Press; 1996. pp. 225–252.
54. Guiguer KRRR, Drimmie R, Power M. Validating methods for measuring  $\delta^{18}\text{O}$  and  $\delta^{13}\text{C}$  in otoliths from freshwater fish. *Rapid Commun Mass Spectrom*. 2003; 17: 463–471. doi: [10.1002/rcm.935](https://doi.org/10.1002/rcm.935) PMID: [12590395](https://pubmed.ncbi.nlm.nih.gov/12590395/)
55. Matta ME, Orland IJ, Ushikubo T, Helser TE, Black BA, Valley JW. Otolith oxygen isotopes measured by high-precision secondary ion mass spectrometry reflect life history of a yellowfin sole (*Limanda aspera*). *Rapid Commun Mass Spectrom*. 2013; 27: 691–699. doi: [10.1002/rcm.6502](https://doi.org/10.1002/rcm.6502) PMID: [23418148](https://pubmed.ncbi.nlm.nih.gov/23418148/)
56. Kozdon R, Ushikubo T, Kita NT, Spicuzza M, Valley JW. Intratest oxygen isotope variability in the planktonic foraminifer *N. pachyderma*: real vs. apparent vital effects by ion microprobe. *Chem Geol*. 2009; 258: 327–337.
57. Kita NT, Ushikubo T, Fu B, Valley JW. High precision SIMS oxygen isotope analysis and the effect of sample topography. *Chem Geol*. 2009; 264: 43–57. doi: [10.1016/j.chemgeo.2009.02.012](https://doi.org/10.1016/j.chemgeo.2009.02.012)
58. Kozdon R, Kelly DC, Kita NT, Fournelle JH, Valley JW. Planktonic foraminiferal oxygen isotope analysis by ion microprobe technique suggests warm tropical sea surface temperatures during the Early Paleogene. *Paleoceanography*. 2011; 26: PA3206.
59. Rollion-Bard C, Blamart D, Cuif JP, Juillet-Leclerc A. Microanalysis of C and O isotopes of azooxanthellate and zooxanthellate corals by ion microprobe. *Coral Reefs*. 2003; 22: 405–415.
60. Rasband WS. ImageJ (Internet). Bethesda, Maryland: U.S. National Institutes of Health; 1997. Available: <http://imagej.nih.gov/ij/>.
61. Meyers SR. astrochron: An R package for Astrochronology (Internet). 2014. Available: <http://cran.r-project.org/package=astrochron>.

62. R Core Team. R: A language and environment for statistical computing. R Foundation for Statistical Computing (Internet). Vienna, Austria; 2014. Available: <http://www.R-project.org/>.
63. Orland IJ, Bar-Matthews M, Kita NT, Ayalon A, Matthews A, Valley JW. Climate deterioration in the Eastern Mediterranean as revealed by ion microprobe analysis of a speleothem that grew from 2.2 to 0.9 ka in Soreq Cave, Israel. *Quat Res.* 2009; 71: 27–35. doi: [10.1016/j.yqres.2008.08.005](https://doi.org/10.1016/j.yqres.2008.08.005)
64. Valley JW, Kita NT. In situ oxygen isotope geochemistry by ion microprobe. In: Fayek M, editor. *MAC Short Course: Secondary Ion Mass Spectrometry in the Earth Sciences.* 2009. pp. 19–63.
65. Orland IJ. Seasonality from speleothems: High-resolution ion microprobe studies at Soreq Cave, Israel. Ph.D. Thesis, University of Wisconsin—Madison; 2012.
66. Friedmann I, O'Neil JR. Compilation of stable isotope fractionation factors of geochemical interest. In: Fleischer M, editor. *Data of Geochemistry.* Sixth. Washington, D.C.: U. S. Government Printing Office; 1977.
67. Kim S-T, Mucci A, Taylor BE. Phosphoric acid fractionation factors for calcite and aragonite between 25 and 75°C: Revisited. *Chem Geol.* 2007; 246: 135–146. doi: [10.1016/j.chemgeo.2007.08.005](https://doi.org/10.1016/j.chemgeo.2007.08.005)
68. Linzmeier BJ. Depth migratory behavior elucidated by ion microprobe analysis of  $\delta^{18}\text{O}$  within *Nautilus macromphalus* shell aragonite. M.S. Thesis, University of Wisconsin—Madison; 2012.
69. Cavosie AJ, Valley JW, Wilde SA, others. Magmatic  $\delta^{18}\text{O}$  in 4400–3900 Ma detrital zircons: A record of the alteration and recycling of crust in the Early Archean. *Earth Planet Sci Lett.* 2005; 235: 663–681.
70. Kozdon R, Kelly DC, Kitajima K, Strickland A, Fournelle JH, Valley JW. In situ  $\delta^{18}\text{O}$  and Mg/Ca analyses of diagenetic and planktic foraminiferal calcite preserved in a deep-sea record of the Paleocene-Eocene thermal maximum. *Paleoceanography.* 2013; 28: 517–528. doi: [10.1002/palo.20048](https://doi.org/10.1002/palo.20048)
71. Kampstra P, Kampstra MP. Package “beanplot.” 2014; Available: <http://cran-mirror.cs.uu.nl/web/packages/beanplot/beanplot.pdf>.
72. Cochran JK, Landman NH. Radiometric determination of the growth rate of *Nautilus* in nature. *Nature.* 1984; 308: 725–727. doi: [10.1038/308725a0](https://doi.org/10.1038/308725a0)
73. Saunders WB. Natural rates of growth and longevity of *Nautilus belauensis*. *Paleobiology.* 1983; 9: 280–288.
74. Hamada T, Mikami S, Okutani T. Experience with aquarium rearing of *Nautilus* in Japan. In: Saunders W, Landman N, editors. *Nautilus: The Biology and Paleobiology of a Living Fossil.* Plenum Press. New York; 1987. pp. 579–583.
75. Kita NT, Sobol PE, Kern JR, Lord NE, Valley JW. UV-light microscope: improvements in optical imaging for a secondary ion mass spectrometer. *J Anal At Spectrom.* 2015; doi: [10.1039/C4JA00349G](https://doi.org/10.1039/C4JA00349G)
76. Cappa CD. Isotopic fractionation of water during evaporation. *J Geophys Res.* 2003; 108. doi: [10.1029/2003JD003597](https://doi.org/10.1029/2003JD003597)
77. Landman NH, Druffel ERM, Cochran JK, Donahue DJ, Jull AJT. Bomb-produced radiocarbon in the shell of the chambered *Nautilus*: rate of growth and age at maturity. *Earth Planet Sci Lett.* 1988; 89: 28–34. doi: [10.1016/0012-821X\(88\)90030-1](https://doi.org/10.1016/0012-821X(88)90030-1)
78. Ward PD. Periodicity of chamber formation in chambered cephalopods: Evidence from *Nautilus macromphalus* and *Nautilus pompilius*. *Paleobiology.* 1985; 11: 438–450.
79. Fatherree JW, Harries PJ, Quinn TM. Oxygen and carbon isotopic “dissection” of *Baculites compressus* (Mollusca: Cephalopoda) from the Pierre Shale (upper Campanian) of South Dakota; Implications for paleoenvironmental reconstructions. *PALAIOS.* 1998; 13: 376–385.
80. Stevens K, Mutterlose J, Wiedenroth K. Stable isotope data ( $\delta^{18}\text{O}$ ,  $\delta^{13}\text{C}$ ) of the ammonite genus *Simbirskites*—implications for habitat reconstructions of extinct cephalopods. *Palaeogeogr Palaeoclimatol Palaeoecol.* 2015; 417: 164–175. doi: [10.1016/j.palaeo.2014.10.031](https://doi.org/10.1016/j.palaeo.2014.10.031)
81. Lukeneder A. Ammonoid habitats and life history. In: Klug C, Korn D, Baets KD, Kruta I, Mapes RH, editors. *Ammonoid Paleobiology: From anatomy to ecology.* Springer Netherlands; 2015. pp. 689–791. Available: [http://link.springer.com/chapter/10.1007/978-94-017-9630-9\\_18](http://link.springer.com/chapter/10.1007/978-94-017-9630-9_18).
82. Moriya K. Isotope signature of ammonoid shells. In: Klug C, Korn D, Baets KD, Kruta I, Mapes RH, editors. *Ammonoid Paleobiology: From anatomy to ecology.* Springer Netherlands; 2015. pp. 793–836. Available: [http://link.springer.com/chapter/10.1007/978-94-017-9630-9\\_19](http://link.springer.com/chapter/10.1007/978-94-017-9630-9_19).
83. McConnaughey T.  $^{13}\text{C}$  and  $^{18}\text{O}$  isotopic disequilibrium in biological carbonates: I. Patterns. *Geochim Cosmochim Acta.* 1989; 53: 151–162. doi: [10.1016/0016-7037\(89\)90282-2](https://doi.org/10.1016/0016-7037(89)90282-2)
84. Basil JA, Hanlon RT, Sheikh SI, Atema J. Three-dimensional odor tracking by *Nautilus pompilius*. *J Exp Biol.* 2000; 203: 1409–1414. PMID: [10751156](https://pubmed.ncbi.nlm.nih.gov/10751156/)
85. Meisel DV, Byrne RA, Kuba M, Mather J, Ploberger W, Reschenhofer E. Contrasting activity patterns of two related octopus species, *Octopus macropus* and *Octopus vulgaris*. *J Comp Psychol.* 2006; 120: 191–197. doi: [10.1037/0735-7036.120.3.191](https://doi.org/10.1037/0735-7036.120.3.191) PMID: [16893256](https://pubmed.ncbi.nlm.nih.gov/16893256/)

86. Wilkinson BH, Ivany LC. Paleoclimatic inference from stable isotope profiles of accretionary biogenic hardparts—a quantitative approach to the evaluation of incomplete data. *Palaeogeogr Palaeoclimatol Palaeoecol.* 2002; 185: 95–114. doi: [10.1016/S0031-0182\(02\)00279-1](https://doi.org/10.1016/S0031-0182(02)00279-1)
87. Ward PD, Martin AW. Depth Distribution of *Nautilus pompilius* in Fiji and *Nautilus macromphalus* in New Caledonia. *The Veliger.* 1980; 22: 259–264.
88. Ward PD, Martin AW. On the buoyancy of the pearly *Nautilus*. *J Exp Zool.* 1978; 205: 5–12.
89. Cochran JK, Landman NH, Turekian KK, Michard A, Schrag DP. Paleooceanography of the Late Cretaceous (Maastrichtian) Western Interior Seaway of North America: evidence from Sr and O isotopes. *Palaeogeogr Palaeoclimatol Palaeoecol.* 2003; 191: 45–64. doi: [10.1016/S0031-0182\(02\)00642-9](https://doi.org/10.1016/S0031-0182(02)00642-9)
90. Lécuyer C, Bucher H. Stable isotope compositions of a Late Jurassic ammonite shell: A record of seasonal surface water temperatures in the southern hemisphere? *EEarth Discuss.* 2006; 1: 1–19.
91. Moriya K, Nishi H, Kawahata H, Tanabe K, Takayanagi Y. Demersal habitat of Late Cretaceous ammonoids: Evidence from oxygen isotopes for the Campanian (Late Cretaceous) northwestern Pacific thermal structure. *Geology.* 2003; 31: 167–170.
92. Ritterbush KA, Bottjer DJ. Westermann morphospace displays ammonoid shell shape and hypothetical paleoecology. *Paleobiology.* 2012; 38: 424–446. doi: [10.1666/10027.1](https://doi.org/10.1666/10027.1)
93. Westermann GEG. Ammonoid life and habitat. In: Landman NH, Tanabe K, Davis RA, editors. *Ammonoid Paleobiology.* New York: Plenum Press; 1996. pp. 607–707.